A Mathematical Model of a River-Shallow Sea System used to Investigate Tide, Surge and their Interaction in the Thames-Southern North Sea Region

Joyce E. Banks

Email alerting service	Receive free email alerts when new articles cite this article - sign up in the box at the top right-hand corner of the article or click **here**

To subscribe to *Phil. Trans. R. Soc. Lond. A* go to: **http://rsta.royalsocietypublishing.org/subscriptions**

[567]

A MATHEMATICAL MODEL OF A RIVER–SHALLOW SEA SYSTEM USED TO INVESTIGATE TIDE, SURGE AND THEIR INTERACTION IN THE THAMES–SOUTHERN NORTH SEA REGION

By JOYCE E. BANKS

Institute of Coastal Oceanography and Tides, Bidston Observatory, Birkenhead, Cheshire

CONTENTS

A mathematical model is used to reproduce tidal and surge motion in the Thames Estuary and the Southern Bight of the North Sea. The model is based on a numerical finite-difference solution of the nonlinear hydrodynamical equations representing motion in the area. The equations are nonlinear in so far as they include quadratic bottom friction and allow for time variations in the total depth of water; the inclusion of advective terms is limited to the river. Solution of the one-dimensional equations for the river and the two-dimensional equations for the sea takes place within a single computational array. The scheme for calculating motion in the sea is similar to that developed by Heaps (1969), and the scheme for the river was developed by Rossiter & Lennon (1965). Tidal and surge motion within the model are reproduced by specifying the initial tidal contours of the sea, the external influences of surge and tidal oscillation along the open sea boundaries, and wind stresses over the sea surface. Computations have been concerned with generating lunar tidal oscillations for the construction of an M_2 co-tidal chart, and investigating the interaction between tides and surges, in this region of shallow waters. The investigation of interaction involved calculating the sea's response to the separate and combined effects of tidal and meteorological forces, whence the effects of a tide on a surge were deduced, possibly for the first time at offshore locations. Computed interaction phenomena for the period of a severe storm surge, 15 to 17 February 1962, were found to accord with the results of Proudman (1955 a, b, 1957) and Rossiter (1961). Agreement between computed sea-level disturbances and actually recorded disturbances for this surge period revealed that the model has good potential for simulating sea level disturbances which occur in nature.

1. Introduction

Concern over the disastrous effects of coastal flooding has instigated a great deal of research into methods of simulating sea levels observed during storms. This research is vital to the design of adequate sea-defence systems and to the forecasting of potentially dangerous surges. A major problem in reproducing the observed sea levels, especially those in shallow waters, is that of properly accounting for the interaction which exists between the meteorologically induced surges and the astronomical tides.

Interaction effects are of hydrodynamical origin (Proudman 1955a). They are caused by the action of friction and variations in the speed of wave propagation which modify a surge in the presence of a tide. Such effects are introduced through the nonlinear terms in the hydro-dynamical equations governing the response of the sea to tidal and meteorological forces. Because of the complexity of these equations when applied to real seas, numerical finite-difference methods (the principles of which are described by Richtmyer 1957) are now frequently used to obtain solutions for tidal and surge motion. Such numerical methods form the basis of mathe-matical models for studying the dynamics of seas and estuaries (see, for example, Heaps 1969). In this paper a mathematical model is developed to simulate observed sea levels in the Thames Estuary and the Southern Bight of the North Sea, a region in which the effects of interaction are of considerable importance due to the concurrence of large tides and large surges. Sea levels of a particular storm surge are determined using the model, and the associated tide–surge inter-actions are discussed in the light of previous explanations of the phenomena as given for example by Proudman (1955a, b, 1957) and Rossiter (1961).

The problem of determining the effects of a tide on a surge has been approached in a variety of ways. It was first considered by Proudman in analytical studies of the propagation of tide and surge along an estuary. Proudman's work yielded a valuable series of formal solutions which revealed the dependence of the interaction on the nonlinear bottom friction, the nonlinear inertia terms and the convergence of the estuary. However the complexity of the nonlinear equations limited the derivation of analytical solutions and subsequent studies have approached the problem either through numerical models or statistical–empirical methods.

One of the first numerical studies was carried out by Rossiter (1961) for the Thames Estuary, utilizing a one-dimensional model. Statistical–empirical methods (Doodson 1924; Corkan 1948; Rossiter 1959; Keers 1968), including the response method (Cartwright 1968; Quraishee 1970), are based on past observations and include interaction effects if a particular state of tide is predicted. In them, in order to determine the effect of the tide on the surge it is necessary to correlate, at the port of interest, the actual surge levels (formed in the presence of the tide) with the hypothetical linear surge (free from tidal effects). The statistical methods of calculating sea level disturbances attach little importance to hydrodynamical considerations. Also because of their dependence on the analysis of observed sea levels they can only reproduce effects at coastal stations where tidal recording devices have been installed; the situation in outer sea regions is undetermined. Numerical models may overcome such deficiencies since they consider the hydrodynamical origins of the interacting waves and also yield information at offshore locations.

In this paper, a numerical model is formulated which represents, in a single computational array, tides and surges in a combined river–shallow sea system. The interplay between tide and surge in an actual period has been reproduced numerically. The objectives have been:

(i) To design a mathematical model of the southern North Sea and Thames Estuary to cal-

culate sea-level disturbances, making allowance for the influx of surge energy across the open-sea boundaries of the area and taking account of surges generated by actual wind fields over the region.

(ii) To use the model to produce a co-tidal chart for the lunar semi-diurnal (M_2) constituent of the tide in the southern North Sea.

(iii) To reproduce sea levels recorded during the period of a major North Sea surge; a satisfactory reproduction would indicate the model's potential in the field of surge forecasting. Also to study the interaction between tide and surge associated with such a major surge, aiming to give a qualitative account of the spatial distribution and time variations of the effect.

The model consists of a one-dimensional river model in combination with a two-dimensional sea model. The system aimed at satisfying a crucial need to interface the two computational meshes so that the mutual interaction between the river and the sea would be incorporated into the calculations. For both river and sea systems the hydrodynamical equations are expressed in nonlinear form. Sea surface elevations and depth-mean currents are evaluated at a series of sections along the river and at an array of points in the sea located at the intersections of a latitude–longitude grid. Coastal and open boundaries of the model follow the boundaries of the southern North Sea as closely as possible.

Computations have yielded the separate and combined effects of tide and surge. In calculating tidal motion, the initial elevations and currents of the sea and river are specified from tidal charts and the tidal oscillations within the model are subsequently generated as co-oscillations with the tides imposed along the open boundaries. Surges, on the other hand, are generated by specifying, at regular intervals of time, both the surge elevations along the open sea boundaries and the actual wind velocities over preselected sub-areas of the model sea – over each of which wind velocity is assumed to be uniform at any time. Sea-level disturbances due to the combined tidal and wind-induced motion are calculated by simultaneously specifying the above conditions. The resulting elevations should be comparable to sea-level observations after removing, from the latter, the effects of changes in barometric pressure assumed to be given by the statical law (Heaps 1967).

Sea-level disturbances of the notorious Hamburg surge (15 to 17 February 1962) have been derived using the model. This surge resulted from a major North Sea storm in which gale force winds raised sea levels in parts of the Southern Bight by over 7 ft. Interactions associated with the surge have been determined as follows. Sea-level disturbances due to (i) tide alone, ζ_T, and (ii) surge alone, ζ_S, were reproduced by the model as were the disturbances due to both tide and surge, ζ_{T+S+I}, the latter containing the effects of interaction and representing the total sea-level disturbance. Removing the tidal contribution (ζ_T) from the total disturbance (ζ_{T+S+I}) revealed the 'surge with interaction' contribution, ζ_{S+I}, so that the distortions of the surge could be seen by comparing ζ_{S+I} with ζ_S. The changing shape of the surge (ζ_{S+I}) profile as it travelled southwards into the shallower water of the southern North Sea has been studied. In the vicinity of the Thames Estuary and off the Dutch coast, where depths are small, double peaks involving friction as the prime cause (Proudman 1955a) became most pronounced and this effect was also most noticeable in the interior of the sea. Along the Thames, the shallowing of the water and the convergence of the estuary caused a fast rise and slow fall in tidal elevations, an increase in their range and also in intensification of the double peaks. At Southend the computed surge residual (ζ_{S+I}) was in good agreement with the observed surge. Also properties of the computed wave along the Thames agreed qualitatively with those derived analytically by Proudman

(1955*a*) and numerically by Rossiter (1961) on the assumption that the tide was of a progressive-wave type. Their results showed that surges occurring on the rising tide were increased as a result of interaction with the tide, while surges occurring at high water were decreased.

This research was started before the British adoption of the SI system of units; thus, unfortunately, the author has used the traditional f.p.s. (+c.g.s.) system. To bring the paper in line with current convention, tables 2 and 3 have been given metric equivalents.

2. FUNDAMENTAL HYDRODYNAMICAL EQUATIONS

Hydrodynamical equations in one and two dimensions are employed for the dynamics of the river and the sea respectively. A single y dimension is involved in the one-dimensional equations; coordinates of latitude and longitude are utilized in the two-dimensional equations. The equations of motion for both river and sea are nonlinear in so far as they include quadratic bottom friction and allow for time variations in the total depth of water. The nonlinearity of the river equations is enhanced by the inclusion of a convective term. The equations are vertically integrated with respect to depth and are therefore independent of the depth coordinate with elevation and components of depth-mean current as the variables for solution.

(a) The sea

The derivation of the hydrodynamical equations for motion in seas has been discussed by Proudman (1953). Linearized forms of the equations in terms of spherical polar coordinates have been given by Heaps (1969). Neglecting vertical acceleration relative to the Earth and all nonlinear accelerations, the equations after vertical integration with respect to depth are:

$$\frac{1}{a\cos\phi}\left\{\frac{\partial U\cos\phi}{\partial\phi}+\frac{\partial V}{\partial\chi}\right\}+\frac{\partial\zeta}{\partial t}=0, \tag{1}$$

$$\frac{\partial U}{\partial t}+\Omega V=-\frac{(h+\zeta)}{\rho a}\frac{\partial p_a}{\partial\phi}-g\frac{(h+\zeta)}{a}\frac{\partial\zeta}{\partial\phi}+\frac{1}{\rho}(F_S-F_B), \tag{2}$$

$$\frac{\partial V}{\partial t}-\Omega U=-\frac{(h+\zeta)}{\rho a\cos\phi}\frac{\partial p_a}{\partial\chi}-\frac{g(h+\zeta)}{a\cos\phi}\frac{\partial\zeta}{\partial\chi}+\frac{1}{\rho}(G_S-G_B), \tag{3}$$

where the notation is as follows:

ϕ,χ	latitude and east-longitude, respectively
t	time
ζ	elevation of the sea surface
(U,V)	total horizontal stream across a vertical line from the sea surface to the sea bottom
(F_S,G_S)	surface stress
(F_B,G_B)	bottom stress
p_a	atmospheric pressure on the sea
h	depth of water below the undisturbed sea surface
ρ	density of water supposed constant and uniform
g	acceleration due to gravity
ω	angular speed of the Earth's rotation
Ω	Coriolis parameter ($=2\omega\sin\phi$)
a	radius of the Earth.

Total stream, surface and bottom stress are here given in terms of components in the directions of increasing ϕ and χ respectively, i.e. to the north and to the east. Depth-mean currents are given by

$$\bar{u} = U/(h+\zeta), \quad \bar{v} + V/(h+\zeta).$$

The present study is concerned with tides and wind-induced surges only. Sea-level displacements due to variations in atmospheric pressure are not included and therefore in the equations of motion $\partial p_a/\partial \phi = \partial p_a/\partial \chi = 0$. Following from empirical formulations, the north and east components of the surface stress may be expressed as:

$$F_S = k_a \rho_a W|W| \cos \beta_s, \quad G_S = k_a \rho_a W|W| \sin \beta_s, \tag{4}$$

where W is the wind velocity, k_a the coefficient of surface friction, ρ_a the density of the air and β_s the clockwise deviation of the wind from a southerly direction.

Bottom stress is expressed in terms of a quadratic law, its components being:

$$F_B = \frac{k_B \rho U|\sqrt{(U^2+V^2)}|}{(h+\zeta)^2}, \quad G_B = \frac{k_B \rho V|\sqrt{(U^2+V^2)}|}{(h+\zeta)^2}, \tag{5}$$

where $\sqrt{(U^2+V^2)}$ is the total stream and k_B the coefficient of bottom friction, taken as 0.0025, the value given by Proudman (1953).

(b) The river

Defant (1961) and Dronkers (1964) discuss the derivation of the one-dimensional equations for a river. Taking y to be the distance along the medial line measured upstream from the mouth the equations may be written

$$\frac{\partial Q}{\partial y} = -\bar{b} \frac{\partial \zeta^{(R)}}{\partial t}, \tag{6}$$

$$\frac{\partial \bar{q}}{\partial t} + \bar{q} \frac{\partial \bar{q}}{\partial y} = -g \frac{\partial \zeta^{(R)}}{\partial y} + \frac{S_S}{\bar{H}\rho'} - \frac{S_B}{\bar{H}\rho'} - \frac{g\bar{H}}{2\rho'} \frac{\partial \rho'}{\partial y}, \tag{7}$$

where
Q is the quadrature $A\bar{q}$,
$\bar{q}$ depth-mean velocity in the direction of y increasing,
A cross-sectional area of the river,
$\zeta^{(R)}$ elevation of the water surface,
$\bar{H}$ mean depth of water,
$\bar{b}$ mean surface breadth,
S_S, S_B surface stress and bottom stress, respectively, in the direction of y increasing,
ρ' depth-mean water density.

Here A, $\bar{H}$ and $\bar{b}$ are functions of position and time satisfying $A = \bar{b}\bar{H}$ while ρ' is assumed to be a function of position only. Rossiter & Lennon (1965) have used the equations as the basis of a mathematical study of motion in the Thames Estuary omitting the surface stress S_S. The latter, by definition, is given by

$$S_S = F_S \sin \theta_R - G_S \cos \theta_R, \tag{8}$$

where θ_R is the inclination of the river course to the east–west line. Over a section of river AB of length δy it is convenient to write

$$S_S = \frac{F_S \mu_{SN} - G_S \mu_{EW}}{\delta y}, \tag{9}$$

where μ_{SN} and μ_{EW} are the projections of AB in the ϕ and $-\chi$ directions and F_S, G_S are values at the mid-point of AB. Bottom stress S_B is assumed to be of the form:

$$S_B = k'\rho'\bar{q}|\bar{q}|, \tag{10}$$

where

$$k' = \frac{gn'^2}{2.22\bar{H}^{\frac{1}{3}}} = \frac{K'}{\bar{H}^{\frac{1}{3}}}, \tag{11}$$

n' being a coefficient of roughness known as the Manning parameter. Optimized values of K' derived by Rossiter & Lennon (1965) for the Thames Estuary have been adopted.

(c) Working equations

It is practically convenient to measure ϕ, χ in degrees, y in miles, t in hours, ζ, $\zeta^{(R)}$, h, $\bar{H}$, $\bar{b}$ in feet, $\bar{q}$, $\bar{u}$, $\bar{v}$ in feet per second S_S, F_S, G_S in dynes per square centimetre, ρ in grams per cubic centimetre. Then incorporating the surface and bottom stress terms into the hydrodynamical equations and taking $a = 6.37 \times 10^3$ km, $g = 32.2$ ft/s², $2\omega = 0.5250\,\text{h}^{-1}$, $\rho = 1.025\,\text{g/cm}^3$ and $k_B = 0.0025$, the equations (6) and (7) and (1) to (3) respectively reduce to

$$\bar{b}\frac{\partial\zeta^{(R)}}{\partial t} = -\alpha_R\frac{\partial Q}{\partial y}, \tag{12}$$

$$\frac{\partial\bar{q}}{\partial t} = -\lambda_R\bar{q}\frac{\partial\bar{q}}{\partial y} - \beta_R\frac{\partial\zeta^{(R)}}{\partial y} - \kappa_R\bar{q}|\bar{q}|\frac{k'}{\bar{H}} + \gamma_R\frac{(\mu_{SN}F_S - \mu_{EW}G_S)}{\bar{H}\delta y} - \frac{\delta_R\bar{H}}{\rho'}\frac{\partial\rho'}{\partial y}, \tag{13}$$

$$\frac{\partial\zeta}{\partial t} = \frac{-\alpha}{\cos\phi}\left\{\frac{\partial U\cos\phi}{\partial\phi} + \frac{\partial V}{\partial\chi}\right\}, \tag{14}$$

$$\frac{\partial U}{\partial t} = -\Omega V - \beta(h+\zeta)\frac{\partial\zeta}{\partial\phi} - \kappa\frac{U|\sqrt{(U^2+V^2)}|}{(h+\zeta)^2} + \gamma F_S, \tag{15}$$

$$\frac{\partial V}{\partial t} = \Omega U - \frac{\beta(h+\zeta)}{\cos\phi}\frac{\partial\zeta}{\partial\chi} - \kappa\frac{V|\sqrt{(U^2+V^2)}|}{(h+\zeta)^2} + \gamma G_S, \tag{16}$$

where

$$\alpha_R = 0.681818, \quad \beta_R = 21.954545, \quad \gamma_R = 3.780503, \quad \delta_R = 10.977273,$$

$$\kappa_R = 3600, \quad \lambda_R = 0.681818, \quad \alpha = 0.00986962, \quad \beta = 0.317802,$$

$$\gamma = 3.780503, \quad \kappa = 9.00 \quad \text{and} \quad \Omega = 0.525\sin\phi.$$

To solve these equations for variations in elevation and flow requires the specification of initial conditions. A suitable starting-point for motion generated by winds alone is to assume that both the river and the sea are initially quiescent whence

$$\zeta = \zeta^{(R)} = U = V = \bar{q} = 0 \quad \text{at} \quad t = 0.$$

For tidal problems the initial conditions of the astronomical tide involving values of $\zeta^{(R)}$ and $\bar{q}$ along the river and ζ, U and V in the sea may be specified.

Elevation and flow must also satisfy conditions which operate at the boundaries. At the head of the river the freshwater flow $\bar{Q}$ is assumed known and constant. Along land boundaries of the sea the component of the flow normal to the boundary must be permanently zero so that

$$U\cos\theta_C + V\sin\theta_C = 0 \quad \text{for all} \quad t \geqslant 0, \tag{17}$$

where θ_C is the angle between the normal to the coast and the direction of increasing ϕ. It

follows that $U = 0$ is the boundary condition on land boundaries lying along parallels of latitude and $V = 0$ is the boundary condition on land boundaries lying along lines of longitude. Along artificial boundaries across the sea called open boundaries, elevation is prescribed as a function of time and position – defining peripheral values of tide and surge. At the mouth of the river, the one-dimensional region meets the two-dimensional region at a point called the 'pivot' and motion at this point is determined by the hydrodynamical equations of both the river and the sea.

3. Finite-difference scheme

(a) Network design

The model called Morass (Model Of River And Shallow Sea) covers the Southern Bight of the North Sea including the Thames Estuary. Figure 1 shows the deployment of grid points over the sea and figure 2 the locations of sections along the River Thames. Over the sea region grid points are positioned at intersections of parallels of latitude equally spaced at $\Delta\phi$ degrees and lines of longitude equally spaced at $\Delta\chi$ degrees. The number of parallels of latitude is denoted by $2p$ and the number of grid points along each parallel by n (figure $3a$). Along the river the grid sections are spaced Δy miles apart along the central channel, the number of sections
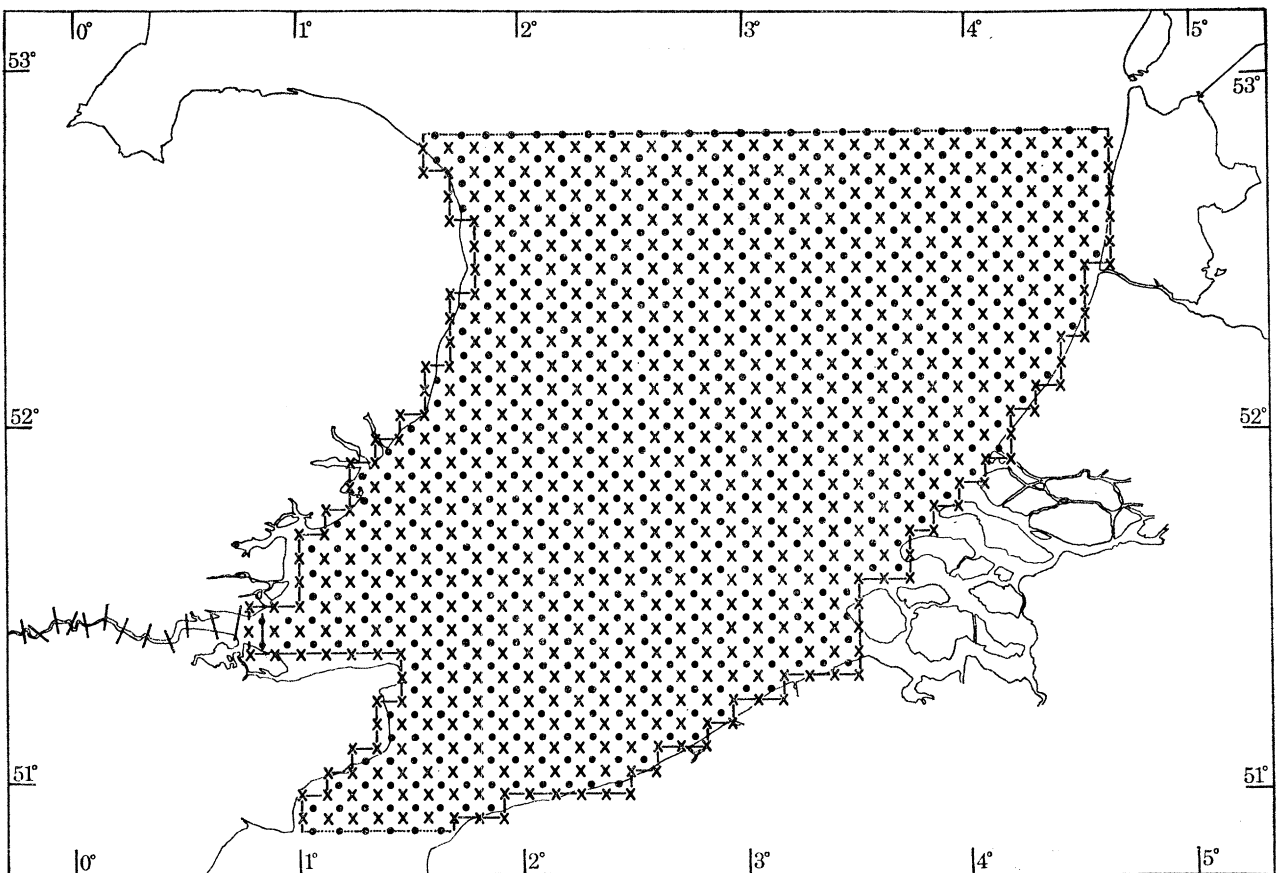

FIGURE 1. Finite-difference grid for the model of the southern North Sea and Thames Estuary. Boundaries of the model marked on the grid: x--x, land boundaries; ●···●, open-sea boundaries. Sea levels are calculated at ●, elevation points and currents at x, stream points; river elevations are calculated at ──, elevation sections.

from the mouth to the head being denoted by $2L$ (figure $3b$). A total size for the sea-river combination is determined by the grid spacings $\Delta\phi$, $\Delta\chi$, Δy and the parameters n, p, L.

Grid points throughout both the river and the sea are denoted either by 'circles' or 'crosses' signifying respectively points at which ζ is evaluated (elevation points) and points at each of
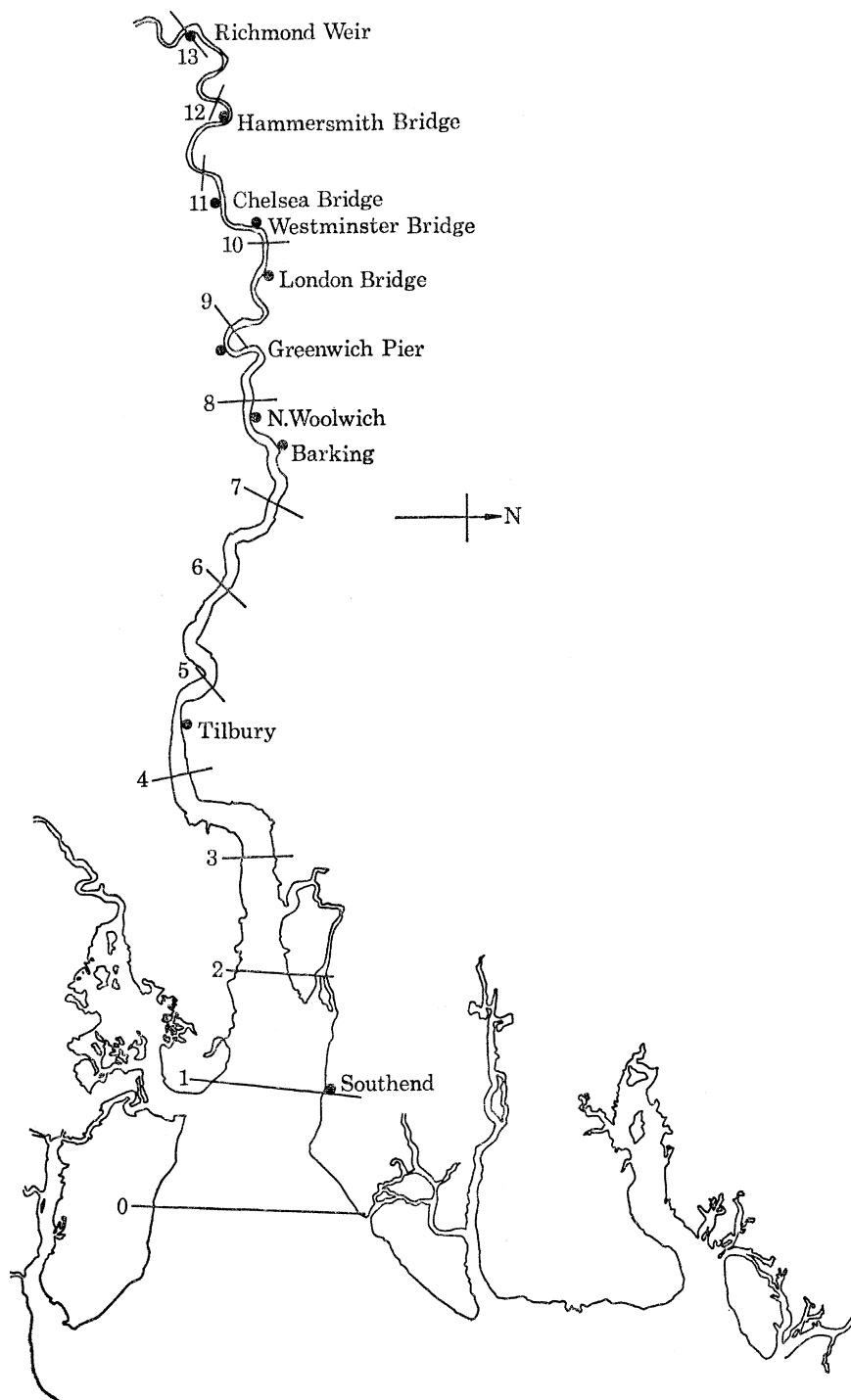
FIGURE 2. Elevation sections along the river Thames. ●, Tide gauge station.

which both U and V are evaluated (stream points, or U, V points). At the stream point junction of the river and the sea models, the pivot, the width of the estuary corresponds to $4\Delta\phi$ degrees (figures 1 and 4). This width represents the limit to which the sea model can extend into the estuary while allowing the necessary space of field variables for the solution of the two-dimensional hydrodynamical equations. Matching currents and elevations around the pivot at points common to both river and sea models is vital and for this reason the sectional spacing in the river and the latitudinal spacing in the sea are made equal. Also a common time step τ is used in the numerical iterations of the river and the sea finite-difference schemes.
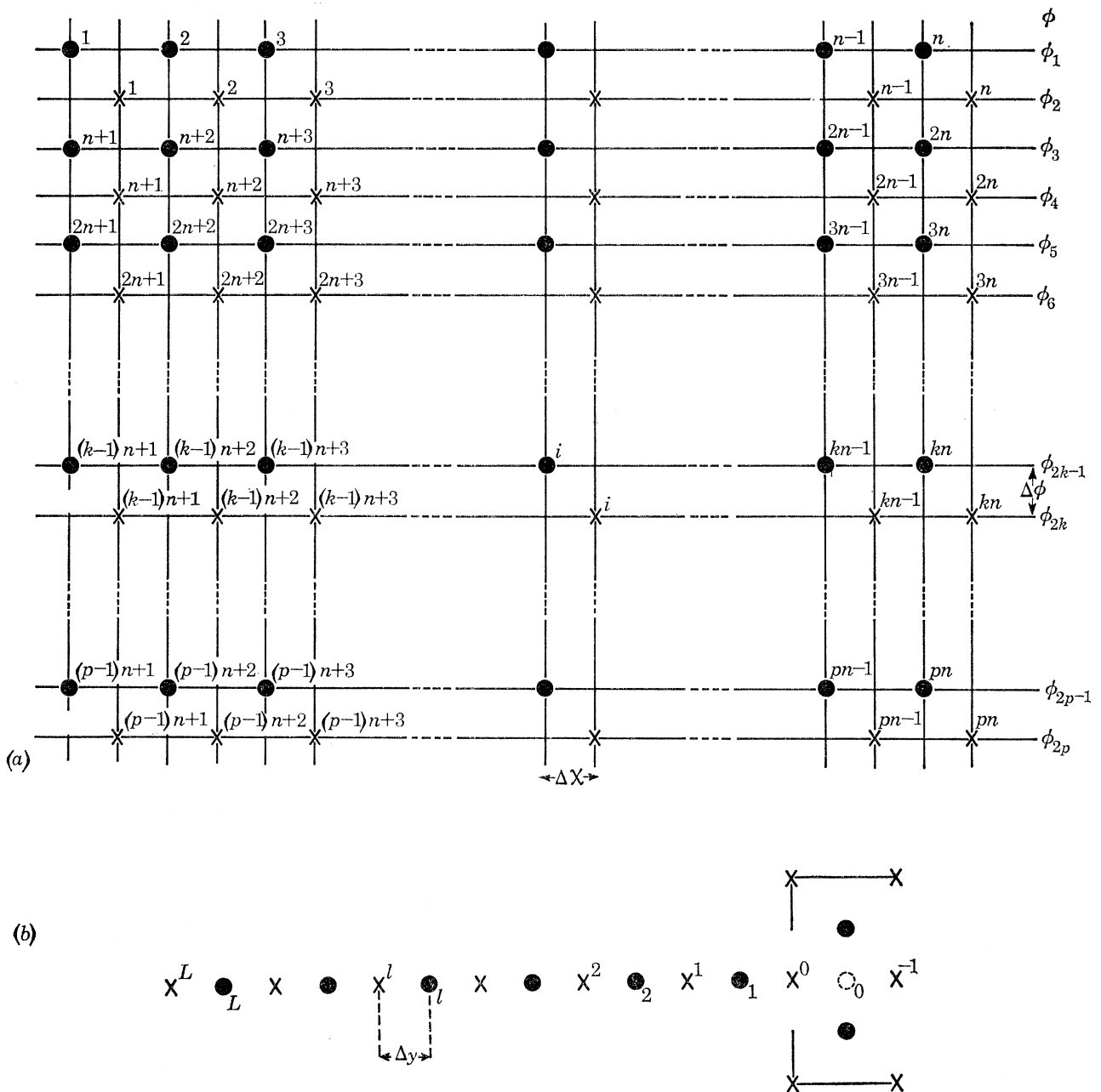

FIGURE 3. (a) Numbering system for the grid points in the sea region; ζ is evaluated at ● points and (U, V) at × points. (b) Numbering system for the river sections; $\zeta^{(R)}$ is evaluated at ● and $\bar{q}$ at × points. The pivotal point is ×⁰.

Current $\bar{q}$ and elevation $\zeta^{(R)}$ sections occur alternately along the river (figure $3b$). Each set of sections is numbered serially $l = 0, 1, 2, 3, \ldots, 13$ in the direction of increasing y from the pivot at the mouth ($l = 0$) to Richmond at the head ($l = 13$). At current section l, $\bar{q} = \bar{q}_l$ while at elevation section l, $\zeta^{(R)} = \zeta_l^{(R)}$. The spacing between successive elevation or current sections is
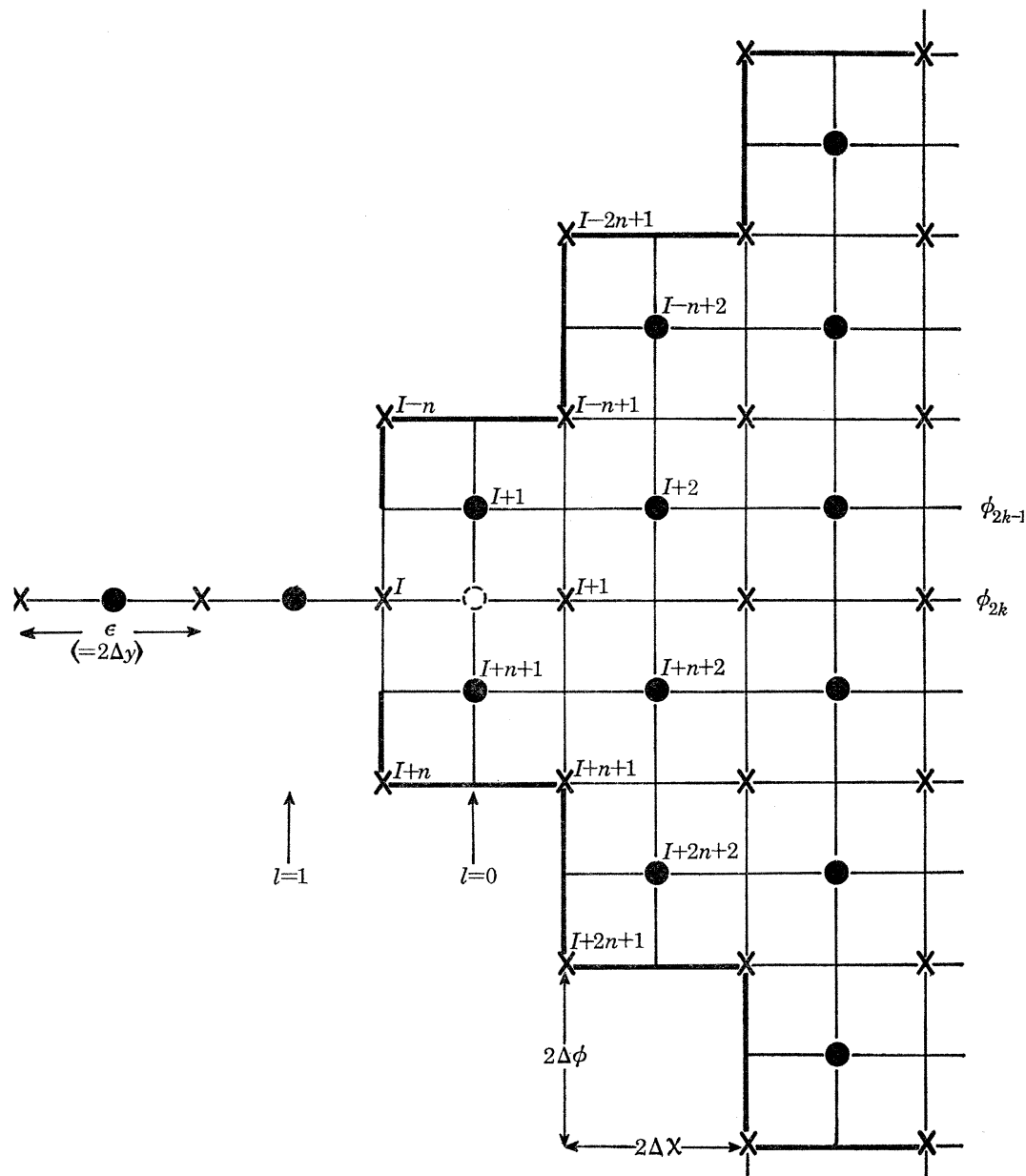

FIGURE 4. Plan-form diagram of river–sea connexion showing the grid points surrounding the pivot I.

denoted by ϵ ($= 2\Delta y$). The present model is based on the finite-difference scheme devised by Rossiter & Lennon (1965) and therefore the same sectional spacing $\epsilon = 4.89$ miles was chosen so that existing river hydrographic data could be used.

Throughout the sea region, stream points and elevation points lie along alternate parallels of latitude and lines of longitude; the arrays of stream and elevation points constitute interlacing

submeshes. Following the method of Heaps (1969), points of each submesh are numbered as demonstrated in figure 3a. The latitudes of the parallels are denoted by ϕ_j where the parallels of the elevation submesh are such that $j = 2k-1$ and those of the stream submesh such that $j = 2k$ $(k = 1, 2, 3, \ldots, p)$. At a stream point i take $U = U_i$, $V = V_i$, $h = h_i$ and $\phi = \phi_{2k}$ and at an elevation point i take $\zeta = \zeta_i$ and $\phi = \phi_{2k-1}$, where $k = 1 + \mathrm{int}\{(i-1)/n\}$, 'int' indicating that the integral part is taken.

In the sea region grid lines of latitude and longitude are oriented from the pivot, the spacings, chosen to give an approximately square mesh, being $\Delta\phi = 2/60$ degrees and $\Delta\chi = 3.4/60$ degrees. The size of $\Delta\chi$ is determined in accordance with the sectional spacing of the river, ϵ, so that at the latitude of the pivot $(\phi = 51° 28.5' \mathrm{N})$ the grid spacing $2\Delta\chi a \cos\phi(\pi/180)$ equals ϵ. As a result, the distance between similar neighbouring points is 4.66 miles on a line of longitude and from 4.74 miles in the north to 4.95 miles in the south on a parallel of latitude.

The rectangular grid system is constructed so that it completely encloses the natural sea region under consideration. Within the network, land boundaries of the sea region are formed from longitudinal or latitudinal lines joining adjacent stream points and open boundaries are formed from such lines joining adjacent elevation points; this yields a zigzag boundary to the model sea.

In superimposing the boundary configuration on to the actual coastline care was taken to ensure that the surface area of the sea contained within the model's boundary was as nearly as possible equal to the actual area of sea bounded by the coastline. The difference between these two surface areas turned out to be three-quarters of the elemental grid area or 0.117 % of the actual sea region. The open boundaries of the model lie along $52°50.5'\mathrm{N}$ in the north and $50°54.5'\mathrm{N}$ in the south. These lines approximately coincide with elevational grid lines of the North Sea model devised by Heaps (1969) along which output of linear surge heights can be employed as input to the present model.

(b) Basic data

Hydrographic data throughout the entire sea–river system is related to Ordnance Datum Newlyn (O.D.N.), which approximates to mean sea level in the outer sea region. At each stream point i of the sea, depths h_{CD} below chart datum were obtained from Admiralty Navigational charts and then adjusted to depths below O.D.N. using the relationship

$$h_i = (h_{\mathrm{CD}} + J_0)_i.$$

Here J_0 denotes the height in feet of O.D.N. above chart datum. In estimating the depth in very shallow waters the minimum value taken for h_{CD} was 6 ft so that $h_i = 6 + J_0$. This was necessary to avoid the possibility of $h_i + \zeta$ becoming zero thereby causing infinities in the frictional terms of equations (15) and (16). To remove any drastic discontinuities, the latitudinal and longitudinal depth profiles were graphically smoothed before extracting the final values of h_i shown in table 1.

(c) Finite-difference equations

The finite-difference scheme for the sea is similar to that described by Lauwerier (1961) and Heaps (1969); however, as an additional feature the present scheme includes certain nonlinear terms in the hydrodynamical equations. As stated earlier, techniques employed by Rossiter & Lennon (1965) are followed in the finite-difference scheme for the river.

Depth, h, components of wind stress, (F, G), and elevation, Z, are defined at every *stream*

JOYCE E. BANKS

TABLE 1. DEPTH h_i BELOW MEAN SEA LEVEL (ft)

28	76	115	112	83	78	88	130	126	118	109	103	101	102	103	101	93	89	88	89	85	83	79	78	80	75	62	46			
18	35	60	79	83	80	114	129	127	123	114	108	103	99	97	95	93	92	91	89	85	82	79	83	80	69	57	32			
	16	39	68	85	97	116	125	130	130	122	112	106	112	106	97	95	92	90	88	84	80	78	82	77	64	53	24			
	16	34	67	83	100	118	138	143	138	141	131	113	120	113	100	97	84	86	90	84	77	75	70	67	58	47	12			
		32	71	83	100	123	142	149	137	127	124	122	125	122	98	90	83	81	84	81	75	71	65	62	54	42	16			
		31	82	101	113	130	139	141	132	122	118	119	123	119	96	88	86	83	78	73	71	69	65	59	51	39	18			
	10	41	91	109	121	130	135	136	130	120	111	106	107	106	88	87	91	90	73	68	68	68	65	58	48	36				
	10	65	91	104	121	130	133	135	132	125	112	110	109	110	88	82	77	72	69	68	68	67	63	56	45	14				
	27	75	92	106	121	136	136	130	130	133	133	122	112	122	91	84	76	74	75	73	70	66	61	54	38	10				
10	49	83	100	119	136	145	145	140	132	128	127	122	115	122	94	89	83	80	77	74	72	66	58	50	16					
11	62	84	101	119	136	144	148	142	133	127	130	128	128	128	110	102	99	89	77	73	75	66	56	34	10					
25	55	75	93	109	127	142	148	141	130	124	129	126	120	126	99	91	84	79	74	71	67	67	46	10						
39	57	74	87	98	120	150	152	144	128	121	117	111	105	111	96	89	83	77	71	65	59	59	40	10						
50	82	111	115	103	112	146	149	134	123	114	101	93	92	93	96	90	84	74	64	52	37	40	18							
52	90	125	107	108	126	150	146	132	123	116	107	98	90	98	86	82	77	68	53	37	19	18	10							
50	83	115	100	113	146	151	140	128	117	109	103	102	96	102	80	83	75	62	41	20	19	10								
38	75	103	104	112	127	135	130	123	116	107	98	102	96	102	83	87	75	30	23	20	11									
53	68	120	125	122	121	117	116	110	101	97	80	85	71	85	81	85	37	13	13											
38	77	129	128	130	118	109	104	94	66	63	93	82	77	82	41	33	25	13	10											
77	99	115	113	118	103	91	93	86	77	75	107	88	80	88	34	23	14													
73	88	118	125	113	97	86	85	81	77	78	80	73	64	73	31	24	20	33												
63	83	115	137	125	105	89	74	66	70	75	66	57	44	57	25	29	33	13												
60	98	114	122	117	107	102	96	77	64	65	57	47	33	47	17	14	13													
67	111	116	112	109	105	92	79	63	48	46	42	31	15	31																
88	111	113	100	103	94	71	64	51	38	28	20	15		15																
121	107	106	107	89	70	65	49	34	29	24	14																			
127	108	90	88	77	73	62	24	16	15																					
136	110	94	71	50	30	20	16	15																						
141	72	27	16																											
89	17																													

point of the model sea. At stream point i their values are denoted by h_i, F_i, G_i and Z_i. A notation $F_{m,i}$ is used to denote $F_i\,(t = m\tau)$, where τ is an elemental time-step and m an integer.

Finite-difference interpretations of the basic differential equations for the sea ((14), (15) and (16)) and river ((12) and (13)) now follow. Central space differences are used throughout for both the river and the sea; however, time differences are central in the river and either forward or backward in the sea.

Within the rectangular grid system an elevation point can be located either outside or within the sea or on its open boundary (figure 1). On the other hand a stream point can lie either outside or within the sea or on a closed boundary where a number of different cases are possible according to the position of the point in relation to the orientation of the boundary in its vicinity. Types of location for elevation and stream points are given integer labels (for example see Heaps 1969).

At a stream point i on latitude ϕ_{2k} lying within the sea, the equations of motion, (15) and (16), represented in finite-difference form are

$$\frac{U_{m+1,i} - U_{m,i}}{\tau} = -\kappa \frac{U_{m,i}|\surd(U^2_{m,i} + V^2_{m,i})|}{(h_i + Z_{m,i})^2} - \Omega_{2k} V_{m,i} - \beta(h_i + Z_{m,i})\frac{D_{m,i}}{2\Delta\phi} + \gamma F_{m,i}, \qquad (18)$$

$$\frac{V_{m+1,i} - V_{m,i}}{\tau} = -\kappa \frac{V_{m,i}|\surd(U^2_{m,i} + V^2_{m,i})|}{(h_i + Z_{m,i})^2} + \Omega_{2k} U_{m,i} - \beta\frac{(h_i + Z_{m,i})}{2\cos\phi_{2k}}\frac{E_{m,i}}{\Delta\chi} + \gamma G_{m,i}, \qquad (19)$$

where (see figure 5a)

$$
\left.
\begin{aligned}
D_{m,i} &= \tfrac{1}{2}[\zeta_i - \zeta_{i+n} + \zeta_{i+1} - \zeta_{i+n+1}]_m, \\
E_{m,i} &= \tfrac{1}{2}[\zeta_{i+1} - \zeta_i + \zeta_{i+n+1} - \zeta_{i+n}]_m, \\
Z_{m,i} &= \tfrac{1}{4}[\zeta_i + \zeta_{i+1} + \zeta_{i+n} + \zeta_{i+n+1}]_m,
\end{aligned}
\right\}
\qquad (20)
$$

and

$$\Omega_{2k} = 2\omega \sin\phi_{2k}.$$

At an elevation point i on latitude ϕ_{2k-1} lying within the boundaries of the sea the equation of continuity (14) is represented by

$$\frac{\zeta_{m+1,i} - \zeta_{m,i}}{\tau} = -\frac{\alpha}{\cos\phi_{2k-1}}\left[\frac{B_{m+1,i}}{2\Delta\phi} + \frac{C_{m+1,i}}{2\Delta\chi}\right], \qquad (21)$$

where (see figure 5b)

$$
\left.
\begin{aligned}
B_{m+1,i} &= \tfrac{1}{2}[U_{i-n}\cos\phi_{2k-2} - U_i\cos\phi_{2k} + U_{i-n-1}\cos\phi_{2k-2} - U_{i-1}\cos\phi_{2k}]_{m+1}, \\
C_{m+1,i} &= \tfrac{1}{2}[V_i - V_{i-1} + V_{i-n} - V_{i-n-1}]_{m+1}.
\end{aligned}
\right\}
\qquad (22)
$$

At an elevation point on an open boundary the ζ_i are specified functions of the time and equation (21) is not applicable.

Equations (18), (19) and (21) are the basic finite-difference equations from which values of the variables at $(m+1)\tau$ are calculated from their earlier values at $m\tau$. These equations may be more conveniently arranged as follows to show this step forward in time:

$$U_{m+1,i} = U_{m,i}\left[1 - \tau\frac{\kappa|\surd(U^2_{m,i} + V^2_{m,i})|}{(h_i + Z_{m,i})^2}\right] - \tau\Omega_{2k}V_{m,i} - \tau\beta(h_i + Z_{m,i})\frac{D_{m,i}}{2\Delta\phi} + \tau\gamma F_{m,i}, \qquad (23)$$

$$V_{m+1,i} = V_{m,i}\left[1 - \tau\frac{\kappa|\surd(U^2_{m,i} + V^2_{m,i})|}{(h_i + Z_{m,i})^2}\right] + \tau\Omega_{2k}U_{m,i} - \tau\frac{\beta(h_i + Z_{m,i})}{2\cos\phi_{2k}}\frac{E_{m,i}}{\Delta\chi} + \tau\gamma G_{m,i}, \qquad (24)$$

$$\zeta_{m+1,i} = \zeta_{m,i} - \frac{\tau\alpha}{\cos\phi_{2k-1}}\left[\frac{B_{m+1,i}}{2\Delta\phi} + \frac{C_{m+1,i}}{2\Delta\chi}\right]. \qquad (25)$$

At a stream point i at the apex of a 270° sector of land

$$U_i = V_i = 0 \qquad (26)$$

for all time, while at a stream point i at the apex of a 90° sector of land (figure 6) equations (23) and (24) are directly applicable. These equations also apply at the pivot i (hereafter denoted by I) marked in figure 4.
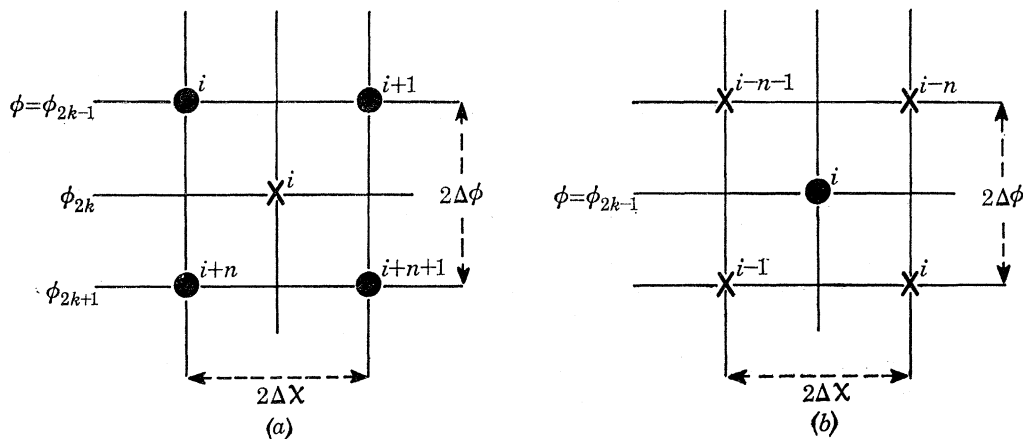

FIGURE 5. Interior grid points. (a) Elevation points surrounding stream point i, (b) stream points surrounding elevation point i.
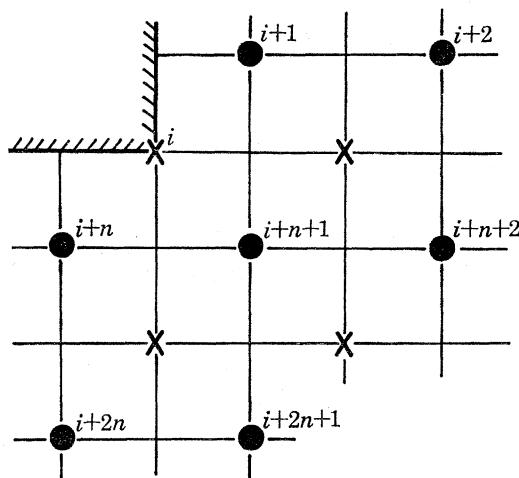

FIGURE 6. Stream point i at a corner formed by a 90° sector of land in the quadrant north to west.

At a stream point i on a longitudinal land boundary (e.g. see figure 7a), V_i is permanently zero and from equation (23),

$$U_{m+1, i} = U_{m, i} \left[1 - \frac{\tau \kappa |U_{m, i}|}{(h_i + Z_{m, i})^2} \right] - \tau \beta (h_i + Z_{m, i}) \frac{D_{m, i}}{2 \Delta \phi} + \tau \gamma F_{m, i}. \qquad (27)$$

Similarly, at a stream point i on a latitudinal land boundary (figure 7b), U_i is permanently zero and from equation (24),

$$V_{m+1, i} = V_{m, i} \left[1 - \frac{\tau \kappa |V_{m, i}|}{(h_i + Z_{m, i})^2} \right] - \tau \frac{\beta (h_i + Z_{m, i})}{2 \cos \phi_{2k}} \frac{E_{m, i}}{\Delta \chi} + \tau \gamma G_{m, i}. \qquad (28)$$

Formulations for D_i, E_i and Z_i in (27) and (28) vary according to the type of location of the stream point relative to the boundary. Thus, derivation of the elevation and elevation gradients at the boundaries is simplified by the introduction of fictitious points shown in figure 8. At these points surrounding the stream point i the elevation will be denoted by μ for points on parallels of the elevation submesh and ν for points on parallels of the stream submesh giving

μ_i for the point due north of i labelled $i+\frac{1}{2}$, $2k-1$ since it lies between elevation points $i, i+1$ on parallel $2k-1$,

μ_{i+n} for the point due south of i, labelled $i+n+\frac{1}{2}$, $2k+1$,

ν_i for the point due west of i, labelled $i-\frac{1}{2}$, $2k$,

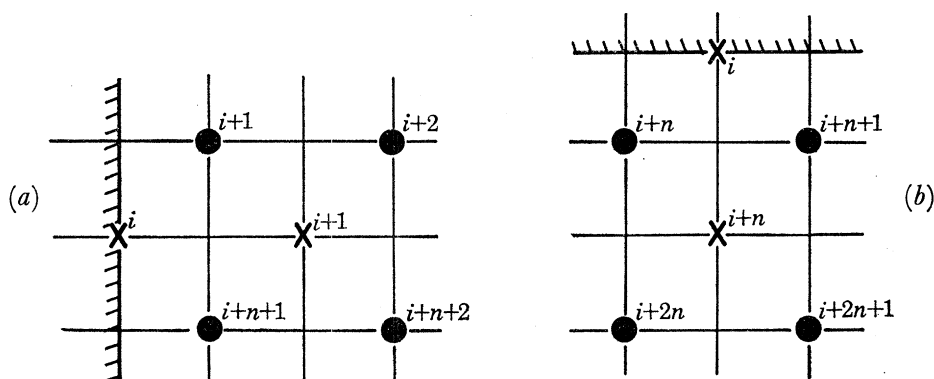ν_{i+1} for the point due east of i, labelled $i+\frac{1}{2}$, $2k$.

FIGURE 7. Stream point i on (a) a longitudinal boundary with land to the west and (b) a latitudinal boundary with land to the north.
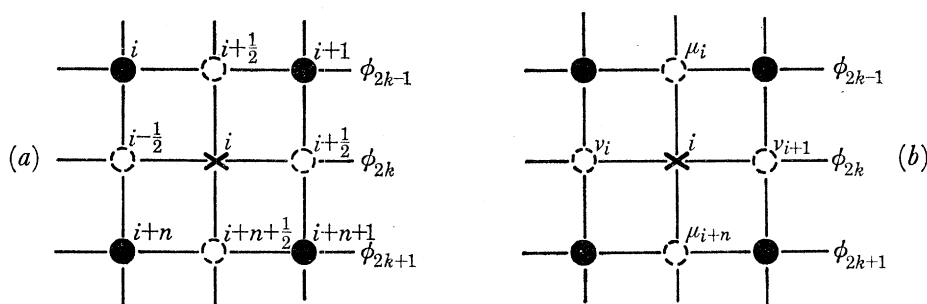

FIGURE 8. (a) Fictitious points $(i+\frac{1}{2}, 2k-1)$, $(i-\frac{1}{2}, 2k)$, $(i+\frac{1}{2}, 2k)$, $(i+n+\frac{1}{2}, 2k+1)$ relative to stream point i. (b) Location of elevations μ_i, ν_i relative to i.

Boundary values of μ_i and ν_i are obtained from the linear extrapolation of adjacent interior elevations. Thus, for example, when land is to the west of a longitudinal boundary as in figure 7a,

$$\mu_i = \tfrac{1}{2}[3\zeta_{i+1} - \zeta_{i+2}], \tag{29}$$

and when land is to the north of a latitudinal boundary as in figure 7b,

$$\nu_i = \tfrac{1}{2}[3\zeta_{i+n} - \zeta_{i+2n}]. \tag{30}$$

Hence at a stream point i lying on a longitudinal boundary

$$Z_i = \tfrac{1}{2}[\mu_i + \mu_{i+n}] \quad \text{and} \quad D_i = \mu_i - \mu_{i+n}. \tag{31}$$

Similarly at a stream point i on a latitudinal boundary

$$Z_i = \tfrac{1}{2}[\nu_i + \nu_{i+1}] \quad \text{and} \quad E_i = \nu_{i+1} - \nu_i. \tag{32}$$

For any stream point i at a corner formed by a 90° sector of land as in figure 6, D_i and E_i are given by

$$Z_i = \tfrac{1}{4}[\mu_i + \mu_{i+n} + \nu_i + \nu_{i+1}], \quad D_i = \mu_i - \mu_{i+n} \quad \text{and} \quad E_i = \nu_{i+1} - \nu_i. \tag{33}$$

At the stream point I, the pivot, the river joins the sea from the west flowing along a parallel of latitude as shown in figure 4. Pivotal point I coincides with the mid-point of current section $l = 0$ so that elevation section 0 is midway between the elevation points $I+1$ and $I+n+1$, hence

$$\begin{aligned}
Z_I &= \tfrac{1}{2}[\zeta_1^{(\mathrm{R})} + \zeta_0^{(\mathrm{R})}] = \tfrac{1}{4}[2\zeta_1^{(\mathrm{R})} + \zeta_{I+1} + \zeta_{I+n+1}], \\
D_I &= \mu_I - \mu_{I+n} = \tfrac{1}{2}[3\zeta_{I+1} - \zeta_{I+2} - 3\zeta_{I+n+1} + \zeta_{I+n+2}], \\
E_I &= \tfrac{1}{2}[\zeta_{I+1} + \zeta_{I+n+1} - 2\zeta_1^{(\mathrm{R})}].
\end{aligned} \right\} \tag{34}$$

and

In the river finite-difference scheme, current calculations are displaced from elevation calculations by a time interval $\tfrac{1}{2}\tau$, the initial currents being specified at $t = -\tfrac{1}{2}\tau$ and elevations at $t = 0$ as shown in figure 9.

Variables $\bar{q}$, Q, A, $\bar{H}$, $\delta\rho'/\rho'$, μ_{SN}, μ_{EW}, F_{S}, G_{S} and k' are defined at *current* section l as $\bar{q}_l$, Q_l, A_l, etc., and variables $\zeta^{(\mathrm{R})}$ and $\bar{b}$ at *elevation* section l as $\zeta_l^{(\mathrm{R})}$ and $\bar{b}_l$. A notation $F_{m,l}$ is used to denote F_l $(t = m\tau)$. At the head of the river the freshwater flow is denoted by $\bar{Q}$.

At a current section l at time $m\tau$ (see figure 9), the equation of motion (13) is interpreted in difference form as

$$\frac{\bar{q}_{m+\frac{1}{2},l} - \bar{q}_{m-\frac{1}{2},l}}{\tau} = -\beta_{\mathrm{R}} \frac{(\zeta_{l+1}^{(\mathrm{R})} - \zeta_l^{(\mathrm{R})})_m}{\epsilon} - \lambda_{\mathrm{R}} \bar{q}_{m,l} \frac{C_{m,l}}{\epsilon} - \kappa_{\mathrm{R}} \bar{q}_{m,l} |\bar{q}_{m,l}| \frac{k_l'}{\bar{H}_{m,l}}$$
$$+ \gamma_{\mathrm{R}} \frac{(\mu_{\mathrm{SN}} F_{\mathrm{S}} - \mu_{\mathrm{EW}} G_{\mathrm{S}})_{m,l}}{\epsilon \bar{H}_{m,l}} - \frac{\delta_{\mathrm{R}} \bar{H}_{m,l}}{\epsilon} \left(\frac{\delta\rho'}{\rho'}\right)_l, \tag{35}$$

where (Rossiter & Lennon 1965):

$$\bar{q}_{m,l} \frac{C_{m,l}}{\epsilon} = \frac{1}{4\epsilon}[\bar{q}_{m+\frac{1}{2},l}(\bar{q}_{m-\frac{1}{2},l+1} - \bar{q}_{m-\frac{1}{2},l-1}) + \tfrac{1}{2}(\bar{q}_{m-\frac{1}{2},l+1}^2 - \bar{q}_{m-\frac{1}{2},l-1}^2)],$$

the product of the currents in the friction term $\bar{q}_{m,l}|\bar{q}_{m,l}|$ is taken as

$$\bar{q}_{m+\frac{1}{2},l}|\bar{q}_{m-\frac{1}{2},l}|$$

and $\delta\rho'/\rho'$, μ_{SN}, μ_{EW}, and k' are allocated values independent of time.

Substitution of the above terms into equation (35) yields

$$\bar{q}_{m+\frac{1}{2},l}\left[1 + \kappa_{\mathrm{R}}\tau|\bar{q}_{m-\frac{1}{2},l}| \frac{k_l'}{\bar{H}_{m,l}} - \frac{\lambda_{\mathrm{R}}\tau}{4\epsilon}(\bar{q}_{l-1} - \bar{q}_{l+1})_{m-\frac{1}{2}}\right]$$
$$= \bar{q}_{m-\frac{1}{2},l} + \beta_{\mathrm{R}}\frac{\tau}{\epsilon}(\zeta_l^{(\mathrm{R})} - \zeta_{l+1}^{(\mathrm{R})})_m + \frac{\lambda_{\mathrm{R}}\tau}{8\epsilon}(\bar{q}_{l-1}^2 - \bar{q}_{l+1}^2)_{m-\frac{1}{2}}$$
$$+ \gamma_{\mathrm{R}}\frac{\tau}{\epsilon}\left(\frac{\mu_{\mathrm{SN}}F_{\mathrm{S}} - \mu_{\mathrm{EW}}G_{\mathrm{S}}}{\bar{H}}\right)_{m,l} - \delta_{\mathrm{R}}\frac{\tau}{\epsilon}\bar{H}_{m,l}\left(\frac{\delta\rho'}{\rho'}\right)_l, \tag{36}$$

where $\bar{H}_{m,l}$ depends on the elevation at current section l at time $m\tau$ taken as $\tfrac{1}{2}[\zeta_{m,l}^{(\mathrm{R})} + \zeta_{m,l+1}^{(\mathrm{R})}]$.

When utilizing the above equation to calculate currents at sections 0 and $L-1$, a knowledge of currents at -1 and L respectively is assumed. The former current is obtained by extrapolation as

$$\bar{q}_{-1} = 2\bar{q}_0 - \bar{q}_1 \tag{37}$$

and the latter is obtained from flow at the head in the form $\bar{q}_{\mathrm{L}} = (\bar{Q}/A)_{\mathrm{L}}$, a constant.

At the pivot, current $\bar{q}_{m+\frac{1}{2},0}$ and flow $V_{m,I}$ are independently determined from equations (36) and (24) respectively. By definition the pivot is located where the motion is predominantly one-dimensional and hence the current $\bar{q}_{m+\frac{1}{2},0}$ and the flow $V_{m,I}$ should be compatible and related by the equation

$$V_{m,I} = -\tfrac{1}{2}(\bar{q}_{m+\frac{1}{2},0} + \bar{q}_{m-\frac{1}{2},0})\,(h_I + \tfrac{1}{2}\{\zeta^{(R)}_{m,1} + \zeta^{(R)}_{m,0}\}),$$

KEY

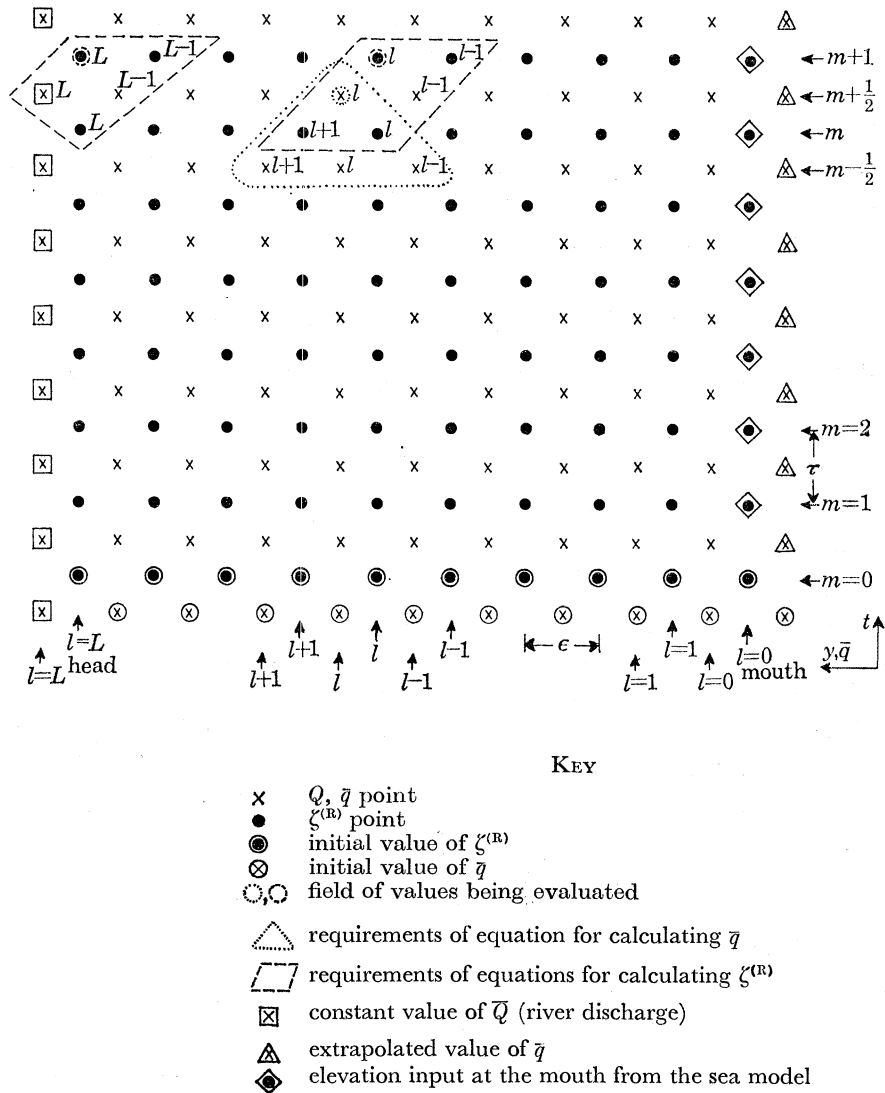|	
$\times$	$Q, \bar{q}$ point
$\bullet$	$\zeta^{(R)}$ point
$\circledcirc$	initial value of $\zeta^{(R)}$
$\otimes$	initial value of $\bar{q}$
$\bigcirc, \mathbin{\text{O}}$	field of values being evaluated
$\triangle$	requirements of equation for calculating $\bar{q}$
$\square$	requirements of equations for calculating $\zeta^{(R)}$
$\boxtimes$	constant value of $\bar{Q}$ (river discharge)
$\triangle$	extrapolated value of $\bar{q}$
$\diamondsuit$	elevation input at the mouth from the sea model

FIGURE 9. Computational scheme for the river.

where, since the direction of increasing y is opposite to that of increasing χ, $\bar{q}$ and V are opposite in sign. To eliminate any discrepancies between current and flow, the value of $V_{m,I}$ is smoothed in accordance with the values of $\bar{q}_{m+\frac{1}{2},0}$ and $\bar{q}_{m-\frac{1}{2},0}$ as follows:

$$V_{m,I} = \tfrac{1}{2}[V_{m,I} - \tfrac{1}{2}(\bar{q}_{m+\frac{1}{2},0} + \bar{q}_{m-\frac{1}{2},0})\,(h_I + \tfrac{1}{2}\{\zeta^{(R)}_{m,1} + \zeta^{(R)}_{m,0}\})]. \tag{38}$$

At an elevation section l at time $(m+\tfrac{1}{2})\tau$ (see figure 9) the equation of continuity, (12), is replaced by

$$\bar{b}_{m+\frac{1}{2},l}\frac{(\zeta^{(R)}_{m+1,l} - \zeta^{(R)}_{m,l})}{\tau} = -\alpha_R \frac{(Q_{m+\frac{1}{2},l} - Q_{m+\frac{1}{2},l-1})}{\epsilon}.$$

Rearranging this equation yields

$$\zeta^{(R)}_{m+1,l} = \zeta^{(R)}_{m,l} + \frac{\tau}{\epsilon} \frac{\alpha_R}{\bar{b}_{m+\frac{1}{2},l}} [(A\bar{q})_{m+\frac{1}{2},l-1} - (A\bar{q})_{m+\frac{1}{2},l}], \tag{39}$$

where $\bar{b}_{m+\frac{1}{2},l}$ depends on the elevation at elevation section l at time $(m+\frac{1}{2})\tau$ taken as

$$\tfrac{1}{2}[\zeta^{(R)}_{m+1,l-1} + \zeta^{(R)}_{m,l+1}]$$

and $A_{m+\frac{1}{2},l}$ depends on elevation at current section l at time $(m+\frac{1}{2})\tau$ taken as $\tfrac{1}{2}[\zeta^{(R)}_{m+1,l} + \zeta^{(R)}_{m,l+1}]$. Since $A_{m+\frac{1}{2},l}$ requires a knowledge of $\zeta^{(R)}_{m+1,l}$ before it has been calculated an iterative process is used with equation (39) first taking $\zeta^{(R)}_{m+1,l-1}$ to approximate to $\zeta^{(R)}_{m+1,l}$ in obtaining $A_{m+\frac{1}{2},l}$, and then finding successive values of $\zeta^{(R)}_{m+1,l}$ and $A_{m+\frac{1}{2},l}$ in a converging sequence.

Before equations (36) and (39) can be solved, elevations and velocities must be known at an array of points shown in figure 9. This figure reveals that at the head of the river an amendment to the equation for the elevation at section L is required, namely

$$\zeta^{(R)}_{m+1,L} = \zeta^{(R)}_{m,L} + \frac{\tau}{\epsilon} \frac{\alpha_R}{\bar{b}_{m+\frac{1}{2},L}} [(A\bar{q})_{m+\frac{1}{2},L-1} - \bar{Q}], \tag{40}$$

where since $\zeta^{(R)}_{m,L+1}$ is not specified, the breadth $\bar{b}_{m+\frac{1}{2},L}$ is taken to depend only on the elevation $\zeta^{(R)}_{m,L}$.

At the mouth of the river (see figure 4) elevation is defined as

$$\zeta^{(R)}_{m+1,0} = \tfrac{1}{2}[\zeta_{m+1,I+1} + \zeta_{m+1,I+n+1}], \tag{41}$$

an average of the elevations across section 0 as calculated from the sea equations.

Difference equations discussed above form the basis for an iterative procedure yielding elevations and currents throughout the entire sea–river region. Theoretical considerations of these difference equations reveal that the time step and grid size cannot be chosen independently of each other if the system is to be numerically stable.

Stability of the composite finite-difference scheme is based on the Courant, Friedrich & Lewy (1928) criterion for the two-dimensional scheme and the Otter & Day (1960) criterion for the one-dimensional scheme. Thus an appropriate stability criterion is that τ simultaneously satisfies the inequality:

$$\tau < \min \left[\frac{\epsilon}{\sqrt{(g\bar{H}_{max})}}, \quad \frac{\epsilon'}{\sqrt{(2gh_{max})}} \right], \tag{42}$$

where $\qquad \epsilon' = \min(\eta, \xi), \quad \eta = 2a \cos\phi \, \Delta\chi(\pi/180), \quad \xi = 2a \, \Delta\phi(\pi/180);$

h_{max} is the maximum depth below mean sea level that occurs in the two-dimensional region and $\bar{H}_{max}$ the maximum depth which may feasibly exist in the river.

In the one-dimensional system $\epsilon = 4.89$ miles and $\bar{H}_{max} = 50$ ft and thus for stability τ must be less than 11 min. In the two-dimensional case $\min(\xi, \eta) = 4.66$ miles and $h_{max} = 160$ ft so that τ is required to be less than 4 min. To ensure the stability of the combined system the time step τ of the iterative procedure was taken as 3 min. Convergence of the computations with respect to time step length was established in early tests on the model when a comparison of results using (a) the 3 min time step and (b) a 5 min time step, showed good and rapid convergence.

(d) Evaluation of currents and elevations

To start the iterative procedure, river currents at time $-\tfrac{1}{2}\tau$ together with river elevations and sea elevations and flows at time zero are specified at their respective grid points of the model as shown in figure 10. Assuming that values of $\bar{q}(\{m-\tfrac{1}{2}\}\tau)$ and $\zeta^{(R)}$, ζ, U, $V(m\tau)$ have been calculated

and F_S, $G_S(m\tau)$ have been specified, their values, after a further time step τ, are obtained from the following sequence of calculations:

(1) River currents $\bar{q}_{m+\frac{1}{2},l}$ are determined for all sections of the river from equation (36) when $l \geqslant 0$ and from equation (37) when $l = -1$.
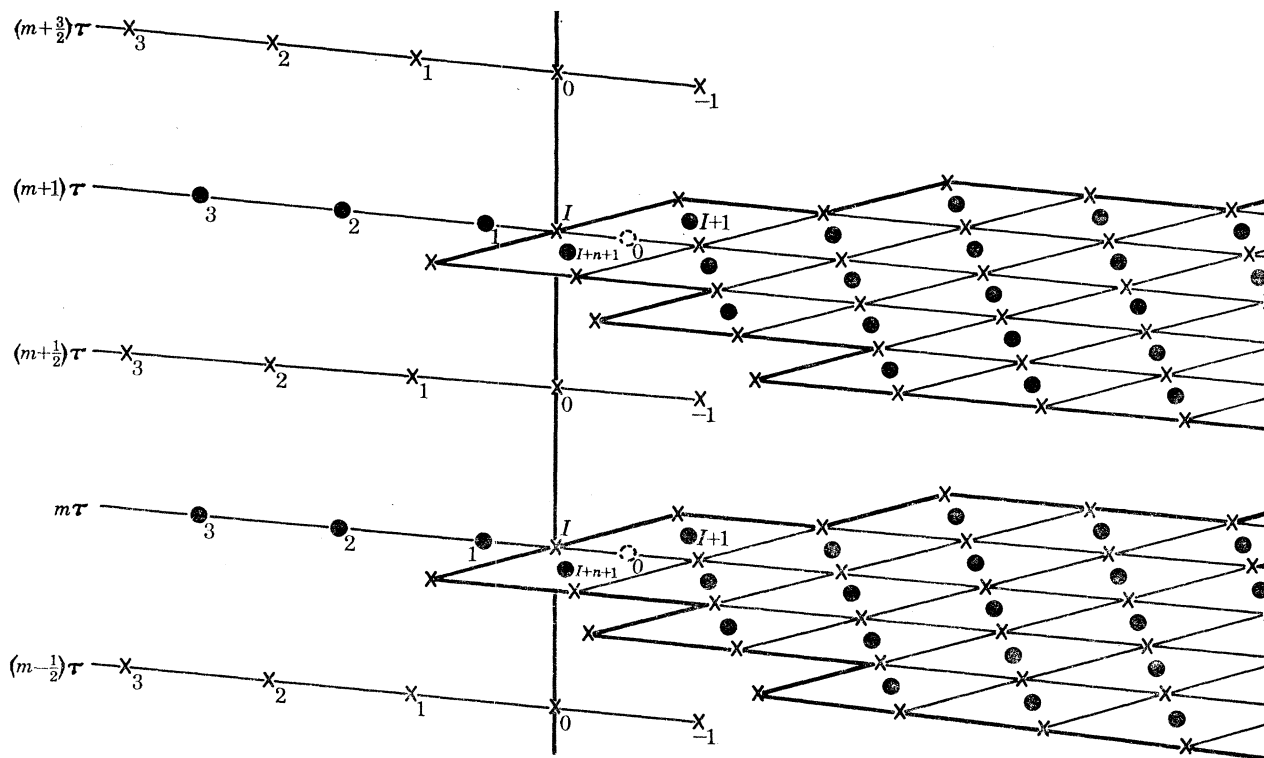

FIGURE 10. Composite computational scheme.

(2) For each stream point i, using equations appropriate to its location, evaluations are made of:

(i) elevation $Z_{m,i}$ from equations (20), (31), (32) or (33);

(ii) depth–mean velocities $U_{m,i}/(h_i + Z_{m,i})$ and $V_{m,i}/(h_i + Z_{m,i})$ knowing $Z_{m,i}$ from (i) above;

(iii) $D_{m,i}$ and $E_{m,i}$ from equations (20), (31), (32) or (33);

(iv) stream flows $U_{m+1,i}$ and $V_{m+1,i}$ from equations (23), (24), (26), (27) or (28).

(3) For each elevation point i within the sea $B_{m+1,i}$ and $C_{m+1,i}$ are calculated from equation (22) and subsequently employed to find $\zeta_{m+1,i}$ from equation (25).

(4) At open boundary points, the $\zeta_{m+1,i}$ are determined as functions of the time and of the position of the point on the boundary; they are calculated independently of the neighbouring internal field values.

(5) Components of the wind F_S, $G_S(\{m+1\}\tau)$ are specified and assumed constant over each successive time interval $(m+1)\tau \leqslant t < (m+2)\tau$.

(6) Smoothing of the stream flow at the pivot now necessitates a calculation of $\bar{q}_{m+\frac{3}{2},0}$ and then a reassessment of certain variables as follows:

(i) $\zeta^{(R)}_{m+1,0}$ is found from (41) and then $\zeta^{(R)}_{m+1,1}$ from (39).

(ii) Current at the pivot $\bar{q}_{m+\frac{3}{2},0}$ is determined from (36).

(iii) Stream flow $V_{m+1,I}$ is revised using (38). Consequently $\zeta_{m+1,I+1}$ and $\zeta_{m+1,I+n+1}$ must be redetermined from equation (25).

(7) Elevation at the mouth of the river $\zeta_{m+1,0}^{(R)}$ is determined from equation (41).

(8) Elevations along the river $\zeta_{m+1,l}^{(R)}$ are determined from equation (39) for $0 < l < L$ and $\zeta_{m+1,L}^{(R)}$ is found from equation (40).

The transformation from $\bar{q}(\{m - \frac{1}{2}\}\tau)$ and $\zeta^{(R)}$, ζ, U, $V(m\tau)$ to $\bar{q}(\{m + \frac{1}{2}\}\tau)$ and $\zeta^{(R)}$, ζ, U, $V(\{m+1\}\tau)$ is therefore accomplished. Successive iterations of the above sequence of calculations for $m = 0, 1, 2, 3, ..., M-1$ yield the numerical distribution of currents and elevations throughout the model at times $\tau, 2\tau, 3\tau, ..., M\tau$, where M is the total number of time steps.

When calculating currents and elevations in steps 2, 3 and 4 above, each type of grid point location requires different equations for determining the field variables. Thus by grouping together points of the same type of location, each point within a group utilizes the same set of equations for calculating variables. Heaps (1969) outlines the method by which the i, k value of each point in the system is related to the group to which the point belongs and the position of the point within its particular group.

For each elevation point of the open boundary, elevations due to both tide and surge are required at every time step of the iterative procedure (step 4 above).

Open boundary tides are given in terms of a series of harmonic constituents. Thus

$$\zeta_i = \sum_{c=1}^{C} J_{c,i} \cos(\sigma_c t - \delta_{c,i}), \tag{43}$$

where i is an open boundary elevation point, and $J_{c,i}$ is the amplitude (in feet), σ_c the angular speed (in degrees per hour), $\delta_{c,i}$ the phase (in degrees), of the cth constituent at i.

Surge elevations are specified at each open boundary point at intervals of $M^*\tau$, where M^* denotes the number of time steps between specifications. In any complete period $M\tau$, consecutive intervals $M^*\tau$ are numbered serially $s^* = 0, 1, 2, 3, ..., S^* - 1$, where s^* denotes the interval $s^*M^*\tau \leqslant t < (s^*+1) M^*\tau$ and $S^*M^* = M$. At each of the M^* time steps of the interval s^*, elevation at open boundary point i is obtained from a four-point Lagrangian interpolation with respect to time between $\zeta_{s^*-1,i}$, $\zeta_{s^*,i}$, $\zeta_{s^*+1,i}$ and $\zeta_{s^*+2,i}$, where $\zeta_{s^*,i}$ denotes the elevation at i at time $s^*M^*\tau$.

Clearly, to obtain elevations over the period $0 \leqslant t \leqslant M\tau$, elevations $\zeta_{s^*,i}$ must be specified for $s^* = -1, 0, 1, 2, 3, ..., S^*, S^* + 1$.

The procedure for specifying the stress F_S, G_S due to the meteorological conditions over the area has been described by Heaps (1969). The model area is divided into sub-areas over each of which, at any one time, the wind is assumed to be uniformly distributed although varying from one sub-area to the next. Such wind conditions are specified at regular time intervals corresponding to an integral number of time steps of the iterative procedure. Both wind speed and direction are assumed constant throughout each interval. Their values are obtained from meteorological charts on the basis of geostrophic winds. During each time interval denoted by s', say, and over each sub-area denoted by sa, say, the wind speed and direction are denoted by $W_{s',sa}$ and $\beta_{s',sa}$ respectively and the resultant wind stress is denoted by $R_{s',sa}$. Components of the surface stress F_S, G_S at stream point i lying in sub-area sa are then given by

$$F_{S_i} = R_{s',sa} \cos\beta_{s',sa} \quad \text{and} \quad G_{S_i} = R_{s',sa} \sin\beta_{s',sa}. \tag{44}$$

Following from Heaps (1969) and Heaps & Ramsbottom (1966), the wind stress (in dynes per square centimetre) is expressed in terms of the surface wind speed using the formula

$$R_{s',sa} = 2.4976 d W_{s',sa}^2, \tag{45}$$

where W is in miles per hour and d the drag coefficient is given by

$$10^3 d = \begin{cases} 0.554 & \text{for} \quad W_{s',sa} \leqslant 11, \\ -0.12 + 0.06124 W_{s',sa} & \text{for} \quad 11 < W_{s',sa} < 43, \\ 2.513 & \text{for} \quad W_{s',sa} \geqslant 43. \end{cases} \tag{46}$$

Matrices $[W_{s',sa}]$ and $[\beta_{s',sa}]$ form the meteorological input data.

4. Tidal computation

Tidal computations performed with the model have been concerned with reproducing the M_2 tide throughout the region of the Thames Estuary and the southern North Sea. Two pieces of computational work have been completed: the first has produced an M_2 co-tidal chart, for comparison with the corresponding long-established Admiralty chart; the second has yielded the M_2 tidal variations associated with the period 15 to 17 February 1962, during which time a major storm surge occurred in the North Sea.

(a) M_2 co-tidal chart

Initial values of elevation and depth–mean current representative of the M_2 tide were determined at appropriate grid points throughout the entire river–sea system. Taking the time origin as that of lunar transit at Greenwich, M_2 elevations throughout the sea at that time were obtained from the British Admiralty Chart no. 301 (1931).

Mean spring tidal currents were used as an approximation to the M_2 currents. From the *Atlas der Gezeitenströme* (Deutsches Hydrographisches Institut 1963) the values of such currents at lunar transit were carefully determined. Both the components of the currents obtained from this atlas and the elevations obtained from the co-tidal charts were smoothed graphically after cross-plotting with respect to latitudinal and longitudinal lines of the finite-difference grid.

Initial river elevations and currents were obtained from Rossiter & Lennon (1965). A mean spring current profile in agreement with the resultant sea current at the pivot was accepted and the corresponding elevations were reduced to achieve consistency with the elevations in the sea.

Starting from the initial values of $\zeta^{(R)}$, $\bar{q}$, ζ, $\bar{u}$ and $\bar{v}$ at lunar transit, M_2 tidal oscillations within the model were generated as co-oscillations with the M_2 tides along the open boundaries. The latter oscillations were defined in terms of the amplitude H and phase g of the M_2 constituent of the tide at each open boundary elevation point. (Values of H and g from the Admiralty co-tidal chart were graphically smoothed after plotting them with reference to latitude along each open boundary; values at each elevation point on the boundary were then determined from the smoothed curve). Tidal amplitude was measured in feet and phase angle, referred to the meridian of Greenwich, in degrees. The speed of the M_2 tide was taken as $30°$/lunar hour ($= \sigma_{M_2}$) since this facilitated the completion of one cycle of the tide in an integral number of iterations. Thus, with $\tau = 0.05$ lunar hour, one cycle covering 12 lunar hours was completed after 240 iterations, with an output of results every lunar hour, i.e. every 20 steps. A further open boundary condition was specified at the head of the Thames where the amount of freshwater inflow (at Richmond) was taken as -1092 ft^3/s, this value being determined from the Thames Conservancy records as applicable to conditions of mean tidal flow.

Tidal computations were performed for a period of 50 lunar hours, the first 24 lunar hours

being regarded as the run-in period necessary to overcome any errors in the specification of initial tidal values.

Appraisal of the calculated lunar tide was achieved in two different ways: first by constructing an M_2 co-tidal chart for comparison with the Admiralty co-tidal chart; secondly, by comparing amplitudes and phases of the observed and computed M_2 tide at selected ports in the southern North Sea and Thames Estuary. Owing to the nonlinearity of the hydrodynamical
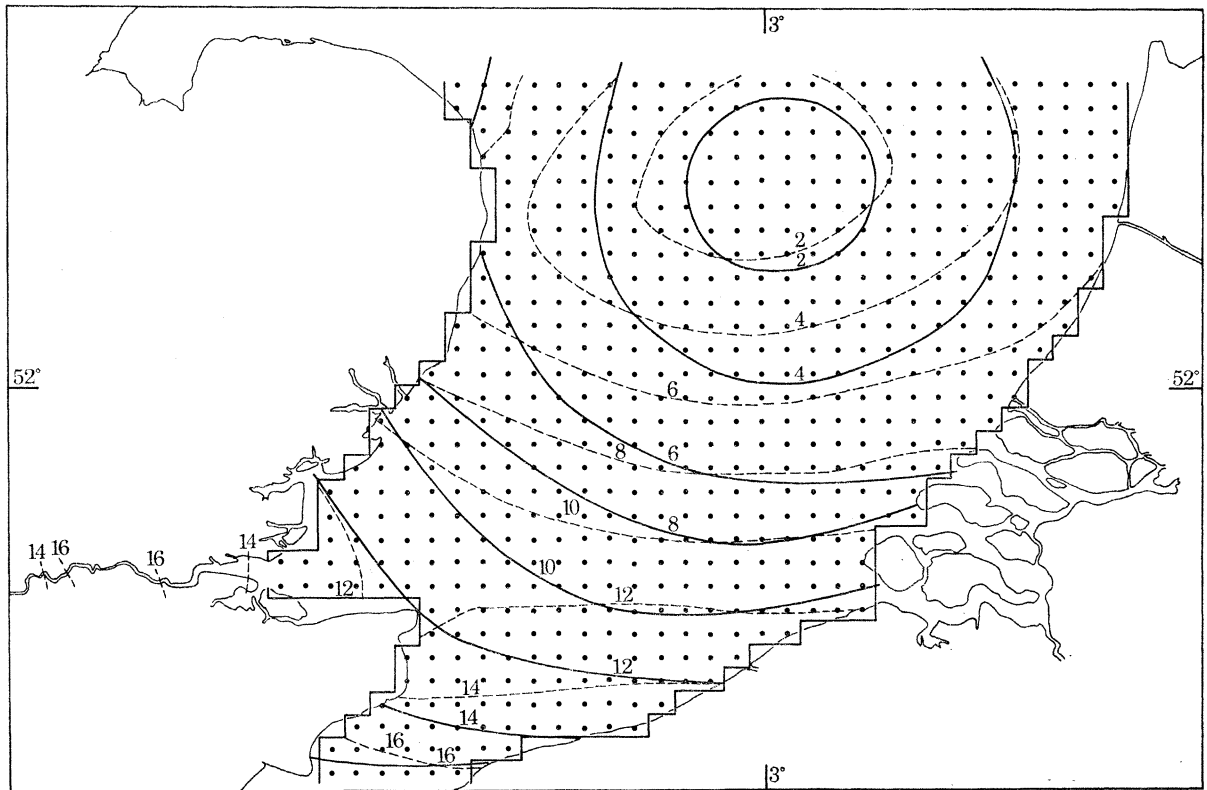

FIGURE 11. Co-range lines for the M_2 tide. ———, Tidal range in feet, taken from Admiralty Chart 301; – –, computed by means of Morass.

equations, the tidal heights generated within the model contained harmonics of the M_2 oscillation as well as M_2 itself. Hence, in order to examine the fundamental semi-diurnal component it was necessary to eliminate the higher-order oscillations from the computed tide. A semi-diurnal band pass filter described by Doodson (1928) was used for this purpose.

To construct the M_2 co-tidal chart from the computed elevations, values of H_{M_2} and g_{M_2} were extracted at points of the elevation submesh lying at the intersections of every third parallel of latitude and every third line of longitude and also at elevation points adjacent to the land boundaries. Thus it was possible to plot the H_{M_2} and g_{M_2} values along each of these lines and so determine, along respective latitudes and longitudes, the locations with a specific range of tide and the locations with a specific phase. By joining the places with an equal range of tide and those with an equal phase, co-range and co-tidal lines were constructed.

A comparison of the computed co-tidal chart with the Admiralty chart (figures 11, 12) reveals the following differences:

(i) Along the open boundaries the values of amplitude and phase from the Admiralty chart

are not identical with those used for generating the tide within the model. The latter were indeed, in the first place, obtained from the Admiralty chart but the subsequent subjection to a smoothing process produced the observed deviations.

(ii) The computed amphidromic centre is only slightly displaced from the Admiralty positioning.

(iii) Computed values of tidal range along the British coast are in satisfactory agreement with chart values; however, along the Dutch coast differences between the two can be as much as 2 ft,
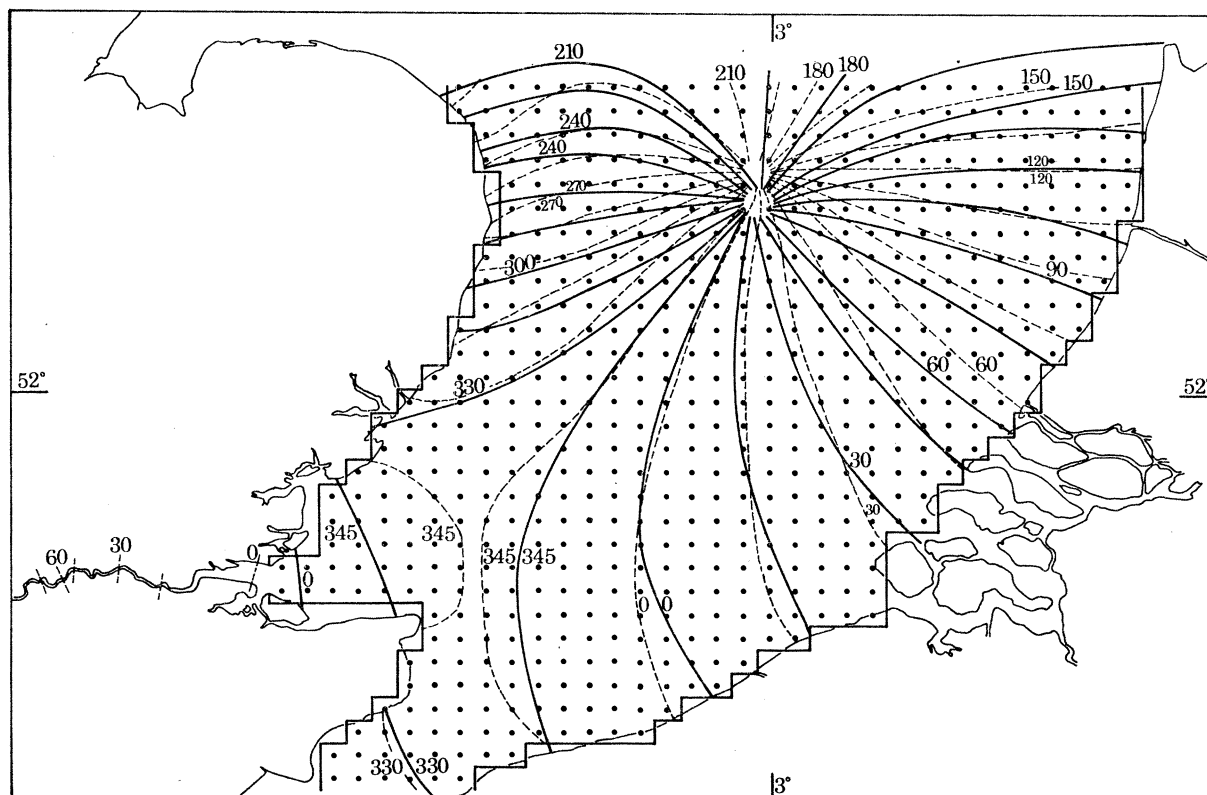
FIGURE 12. Co-tidal lines for the M_2 tide. ——, Phase of tide in degrees, taken from Admiralty Chart 301; – –, computed by means of Morass.

the computed range being the larger. This difference was perhaps in some part due to the specification of the M_2 amplitude near Den Helder where the value given on the Admiralty chart ($H_{M_2} = 3.0$ ft) is higher than that given by I.H.B. (1966) from harmonic analysis ($H_{M_2} = 1.7$ ft). Although the I.H.B. and Admiralty values are in agreement further south along the Dutch coast, this high value for the amplitude of M_2, used as open boundary input to the program, probably contributed to the erroneously increased values of the computed elevations. Another possible contributory factor might have been the exclusion of the Dutch delta region from the Morass model, so that water which should have entered the delta region might instead have contributed to the increase in tidal range.

(iv) The pattern of computed co-tidal lines is in quite good agreement with that of the chart. On the approaches to the Thames the model tide lags behind that in reality. Possibly a faster propagation could be achieved by increasing the depth of water in the outer estuary.

A better assessment of the quality of the results obtained from the model is obtained from

table 2. In this table values of the amplitudes and phases of the computed M_2 tide at selected port locations around the southern North Sea have been extracted from both the computed and the Admiralty co-tidal charts. These values are tabulated alongside values of the M_2 constants obtained from the Institute of Coastal Oceanography and Tides (I.C.O.T.) and I.H.B. analyses of observations. Thus table 2 reveals the differences between the magnitudes of the constants from these three sources.

TABLE 2. COMPARISON OF HARMONIC CONSTANTS FOR M_2

	constants from Admiralty co-tidal chart 301			constants from computed co-tidal chart			constants from analysis		
	amplitude		phase	amplitude		phase	amplitude		phase
name of port	ft	m	deg	ft	m	deg	ft	m	deg
Winterton	3.00	0.91	233.0	3.35	1.02	223.0	3.34	1.02	211.0
Caister	2.90	0.88	247.0	3.00	0.91	234.4	2.92	0.89	225.0
Gorleston	2.90	0.88	264.4	2.69	0.82	251.5	2.43	0.74	241.1
Lowestoft	2.90	0.88	275.6	2.50	0.76	269.0	2.34	0.71	257.5
Southwold	3.14	0.96	297.0	2.65	0.81	302.5	2.51	0.77	283.0
Aldeburgh	3.50	1.07	316.0	3.30	1.01	314.0	2.84	0.87	303.0
Bawdsey	4.30	1.31	327.0	4.20	1.28	330.0	3.63	1.11	315.0
Gunfleet Lighthouse	5.30	1.62	338.0	5.50	1.68	345.0	4.78	1.46	333.0
Harwich	5.10	1.55	329.5	5.00	1.52	338.0	4.33	1.32	328.9
Clacton	5.60	1.71	340.7	5.70	1.74	346.0	4.92	1.50	336.0
Brightlingsea	5.90	1.80	345.0	5.80	1.77	347.0	5.39	1.64	341.0
Margate	6.10	1.86	345.0	5.80	1.77	346.0	5.46	1.66	342.0
Ramsgate	6.17	1.88	344.0	5.95	1.81	344.0	6.09	1.86	338.8
Dover	7.00	2.13	330.0	7.25	2.21	330.0	7.48	2.28	332.9
Calais	7.75	2.36	341.3	7.85	2.39	339.0	7.80	2.38	340.8
Dunkerque	6.75	2.06	352.5	7.53	2.30	356.0	6.91	2.11	353.0
Nieuport	6.17	1.88	359.0	7.08	2.16	3.7	6.10	1.86	359.8
Ostend	5.75	1.75	2.8	6.68	2.04	9.4	5.90	1.80	5.2
Zeebrugge	5.25	1.60	15.0	6.20	1.89	16.0	5.60	1.71	10.0
Flushing	5.10	1.55	26.0	5.88	1.79	27.8	5.64	1.72	31.3
Hook of Holland	2.85	0.87	67.0	3.52	1.07	62.0	2.63	0.80	63.3
Scheveningen	2.77	0.84	78.0	3.20	0.98	72.5	2.40	0.73	73.3
Katjwijk	2.77	0.84	86.2	3.10	0.94	82.5	2.23	0.68	80.3
Ijmuiden	2.75	0.84	110.6	2.90	0.88	105.0	2.23	0.68	105.3
Den Helder	3.00	0.91	150.0	—	—	—	1.74	0.53	158.3

Along the British coast there is little difference in either amplitude or phase between the Morass and Admiralty values. Slightly greater differences exist between values from the model and those from analysis, while the greatest differences are between Admiralty values and values from analysis.

Along the continental coast the reverse is true of the differences in amplitude: the least differences are between the Admiralty and analysed values and the greatest between Morass on the one hand and both Admiralty and analysis on the other. No appreciable differences in phase are exhibited along the continental coast.

Table 2 leads to the conclusion that the model results can hardly be discredited since discrepancies between constants obtained from the model and the Admiralty chart are no worse than discrepancies between the Admiralty and I.H.B. constants.

Values of computed M_2 amplitudes and phases along the Thames Estuary have been plotted

respectively against section number in figure 13. Amplitude, H_{M_2}, increases linearly with distance from the mouth until section 8, thereafter to the head the amplitude decreases. Phase, g_{M_2}, increases from about 0° at Southend to about 85° at Richmond; the progression is steady from Southend at the mouth up to Tower Pier and slower thereafter up to the head. Figure 13 also
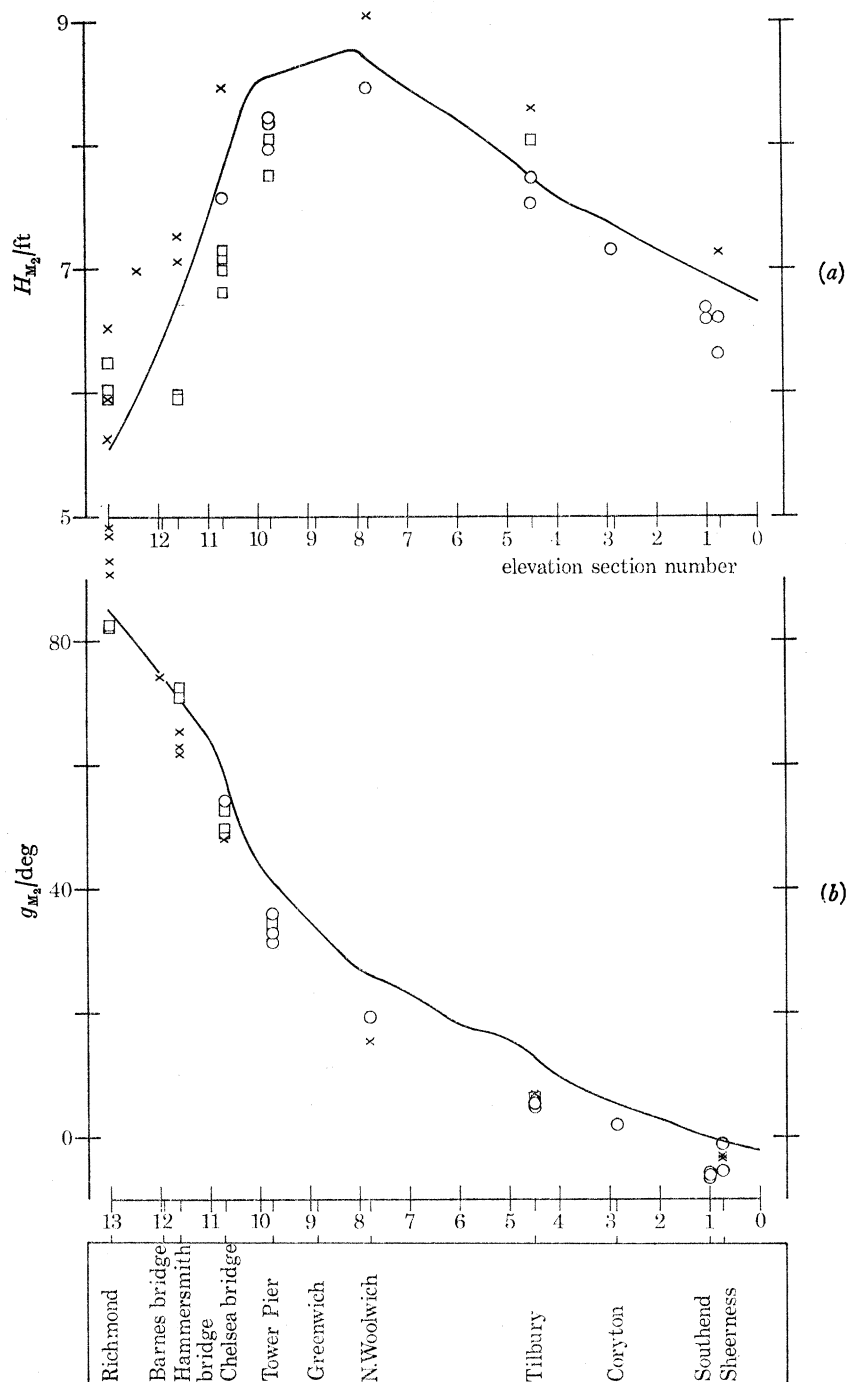

FIGURE 13. (a) Amplitude and (b) phase of the M_2 tide along the Thames. ——, Morass computations; ○, □ from harmonic analyses of observations (○, ~ 1 year; □, ~ 29 days); ×, from non-harmonic time or height differences between standard and secondary ports.

depicts values of H_{M_2} and g_{M_2} obtained from I.C.O.T. analyses of observations at Thames ports. I.C.O.T. harmonic constants at any one place have been derived from hourly observations reduced according to the harmonic method. Those denoted by a circle were derived from observations extending over a period of one year, and those denoted by a square from observations taken over a period of 29 days. Finally, the figure also includes some approximate values of the constants, recorded by a cross, derived from non-harmonic time and height differences between standard and secondary ports. These differences were estimated from British Admiralty Tide Tables for the year of the observations which yielded the standard port constants. At each port the amplitudes and phases deduced from Admiralty Tide Tables and I.C.O.T. analyses exhibit a wide range of values. Amplitudes of the computed oscillations lie well within this range and so were considered to be satisfactory. Computed phases were also acceptable since they were only some 5° greater than the phases deduced from the analyses.

The Morass tide was finally shown to exhibit a close similarity with the tide produced by Rossiter & Lennon (1965) using their well established Thames Estuary model.

Summarizing, tidal heights computed with the model have undergone rigorous examination throughout the entire river–sea region, first, in the main body of the sea, where co-tidal and co-range lines of the computed M_2 tide exhibited favourable agreement with the Admiralty co-tidal chart; secondly, at coastal stations, where amplitudes and phases of the computed tide were compatible with M_2 constituents of observed tides; finally, along the Thames Estuary where the tide computed using Morass was of compatible quality to that produced by the established Thames Estuary model. The above appraisals of the computed tide have proved it to be acceptable overall.

However, because results were influenced by inaccuracies in open boundary data obtained from the Admiralty chart, a method of obtaining an improved specification of open boundary tidal conditions was sought. Offshore values of harmonic constants were available from German (Marineobservatorium Wilhelmshaven 1942) as well as British co-tidal charts. Also it was found that the Dutch Ministry of Defence had derived harmonic constants from offshore observations in the southern North Sea. By collating all these constants, revised open boundary conditions were obtained and, as now described, an attempt was made to improve the reproduction of the M_2 tide.

(b) Lunar tide of 15 to 17 February 1962

This second attempt to simulate a lunar semi-diurnal tide within the model was made for two reasons: (i) to discover whether a significantly closer agreement between observed and computed M_2 amplitudes and phases could be obtained by generating the model tide from an improved specification of open boundary conditions; and (ii) to assess the accuracy with which the model could reproduce lunar tidal variations during an actual period of time, and also to discover how far this computed tide is an approximation to the total observed tide. Attention was focused on the Hamburg surge of 15 to 17 February 1962. Thus by considering the reproduction of the M_2 régime for this period, results became available for later studies of surge–tide interaction as well as answering the questions posed by (i) and (ii) above.

Computations commenced at 00 h 00 of the 13 February so that an adequate run-in period (covering the 13 and 14 February) would be assured. The complete period of computation thus extended over the 5 days 13 to 17 February. Computations were ordered so that recorded fresh-water flows into the river (of the order of 3300 ft³/s) could be specified for each day of the period. The average flow recorded over the 2 days 13 and 14 February was specified for the run-in

period, computed in a single run of the computer program. The rest of the period was divided into three separate runs corresponding to the 15, 16 and 17 February respectively and each of these runs utilized the appropriate daily recorded average of the freshwater flow.

The lunar tidal régime within the model was set up and controlled by the M_2 oscillations along the northern and southern open boundaries as before. At each elevation point of these boundaries, the oscillations were specified in terms of the M_2 harmonic constants:

$$\zeta_{M_2} = J \cos (\sigma_{M_2} t - \delta),$$

where
$$J = f H_{M_2}, \quad \delta = g - V^* - u^*.$$

Here V^* is the phase of the M_2 equilibrium constituent at Greenwich at 00 h 00 13 February 1962,

u^* is the angle representing the nodal variations added to V^*,

g is the phase lag in degrees,

H_{M_2} is the amplitude of the M_2 constituent in feet,

f is the factor representing the nodal variations in the equilibrium amplitude,

σ_{M_2} is the angular speed of M_2 in degrees per hour,

t is the time in solar hours, $t = 0$ representing 00 h 00 13 February 1962.

The values of V^*, u^* and f for 13 February 1962 were extracted from a table of known constants. Amplitudes H and phases g of the M_2 tide were obtainable from three sources, namely German and British co-tidal charts and Dutch analyses of observations covering a period of 1 month taken at several offshore locations. Constants from all three sources were collated and smoothed by constructing contour lines representing $H \sin g$ and $H \cos g$ over the entire southern North Sea. In constructing these smoothed lines from the amalgamated data, most importance was attached to the constants from the Dutch observations since these recorded actual conditions in the interior of the sea. Also good agreement was sought with I.C.O.T. and I.H.B. constants for coastal ports since these had been obtained from analyses of long periods of observations which, in most cases, covered 1 year. Values of H and g at the open boundary points were extracted from the smoothed tidal contours.

Initial values specified in §4a were utilized to define conditions at 00 h 00 on 13 February, the starting-point of the tidal computations for the 5-day period. Inconsistencies of the initial elevations and currents were removed by the 2-day run-in to the calculations. Inspection of the computed elevations and currents showed that they had settled down to a steady oscillation before 00 h 00 on 15 February.

Tidal computations for the complete 5-day period were carried out on the English Electric K.D.F. 9 digital computer at Liverpool University in a total running time of 4 h 30 min. As mentioned in §4a the computed oscillations consisted of a combination of semi-diurnal and higher order constituents of the lunar tide, the latter being introduced through the nonlinear terms in the hydrodynamical equations. Thus before amplitudes and phases of the M_2 tide could be determined, they had to be filtered out from the composite computed tidal oscillations. The application of the Doodson method of filtering mentioned in the previous section is a lengthy process and therefore species analyses of the tidal curves were performed using a computer program devised by Murray (1963). This program performs a least squares analysis on any type of tidal data for any number of constituents and was utilized to determine amplitude H and phase g of the M_2 constituent of the tide at various grid points.

Table 3 gives the results of the above analyses at selected grid points adjacent to ports. Names of the ports nearest to the chosen points are also given together with the M_2 amplitudes and phases

TABLE 3. HARMONIC CONSTANTS FOR M_2 AT A NUMBER OF COASTAL GRID POINTS AND AT CORRESPONDING NEARBY PORTS

1	2 computed tide of 15 to 17 February 1962			3 computed tide of §4a			4	5 tide estimated from computed co-tidal chart			6 I.H.B. and I.C.O.T. analyses			7 tide estimated using columns 3 and 5 to correct column 2		
point i	amplitude ft	m	phase deg	amplitude ft	m	phase deg	port (nearest to point)	amplitude ft	m	phase deg	amplitude ft	m	phase deg	amplitude ft	m	phase deg
115	3.01	0.92	235.2	2.97	0.91	236	Caister	3.00	0.91	234.4	2.92	0.89	225.0	3.04	0.93	233.6
221	2.22	0.68	281.8	2.22	0.68	284	Lowestoft	2.50	0.76	269.0	2.34	0.71	257.5	2.50	0.76	266.8
496	4.80	1.46	338.7	4.97	1.51	340	Harwich	5.00	1.52	338.0	4.33	1.32	328.9	4.83	1.47	336.7
565	5.57	1.70	345.4	5.73	1.75	346	Clacton	5.70	1.74	346.0	4.92	1.50	336.0	5.54	1.69	345.4
1	6.67	2.03	357.8	6.90	2.10	0	Southend	6.90	2.10	0.0	6.68	2.04	354.1	6.67	2.03	357.8
10	8.18	2.49	38.4	8.50	2.59	44	Tower Pier	8.56	2.61	41.0	8.17	2.49	32.9	8.24	2.51	35.4
916	7.38	2.25	333.7	7.25	2.21	331	Dover	7.25	2.21	330.0	7.48	2.28	332.9	7.38	2.25	332.7
991	7.97	2.43	343.5	7.80	2.38	339	Calais	7.85	2.39	339.0	7.80	2.38	340.8	8.02	2.44	343.5
961	7.52	2.29	356.9	7.53	2.30	356	Dunkerque	7.53	2.30	356.0	6.91	2.11	353.0	7.52	2.29	356.9
894	6.81	2.08	6.8	6.90	2.10	6	Nieuport	7.08	2.16	3.7	6.10	1.86	359.8	6.99	2.13	4.5
860	6.44	1.96	10.0	6.57	2.00	9	Ostend	6.68	2.04	9.4	5.90	1.80	5.2	6.55	2.00	10.4
793	5.84	1.78	20.7	5.98	1.82	21	Zeebrugge	6.20	1.89	16.0	5.60	1.71	10.0	6.06	1.85	15.7
760	5.78	1.76	26.0	5.93	1.81	26	Flushing	5.88	1.79	27.8	5.64	1.72	31.3	5.73	1.75	27.8
622	4.32	1.32	38.3	4.44	1.35	39	Brouwershaven	4.35	1.33	44.0	3.77	1.15	56.3	4.23	1.29	43.3
486	3.47	1.06	61.0	3.52	1.07	62	Hook of Holland	3.52	1.07	62.0	2.63	0.80	63.3	3.47	1.06	61.0
348	2.95	0.90	80.3	2.99	0.91	83	Katwijk	3.10	0.94	82.5	2.23	0.68	80.3	3.06	0.93	79.8
210	2.63	0.80	104.6	2.82	0.86	109	Ijmuiden	2.90	0.88	105.0	2.23	0.68	105.3	2.71	0.83	100.6

at these ports obtained from analyses of long periods of observations of at least 1 year in length. As shown in figure 14, the locations of selected points and ports seldom coincide and are more often separated by a distance which can be as great as 5 miles. Over the intervening distance, between point and port, some increase or decrease in the amplitudes and phases of the tide can be expected. An estimate of the amount of change may be deduced from the table by inspecting the differences between columns 3 and 5. The estimated change can then be added to the figures
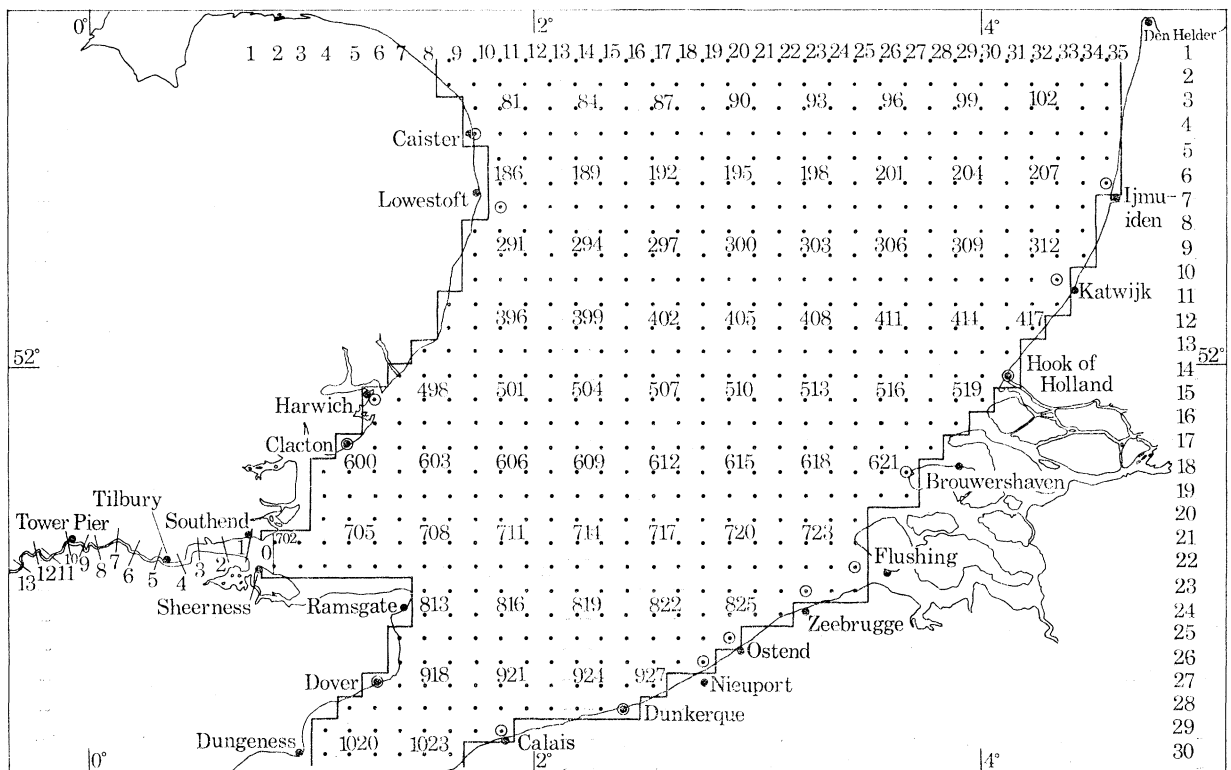
FIGURE 14. Locations of ports relative to Morass elevation points. ⊙, Morass elevation point at which computed elevations are compared with elevations derived from observations at a nearby port.

in column 2 to give an estimate of the 1962 tide at the port (column 7). A comparison of the computed H_{M_2} and g_{M_2} (column 7) with I.H.B. and I.C.O.T. values (column 6) revealed the following improvements over the previous tidal computations (column 3):

1. Computed M_2 amplitudes are slightly improved at most British and continental ports. The maximum discrepancies along the respective coastlines are 0.6 ft at Clacton and 0.9 ft at Nieuport.

2. (i) Computed phases at British ports reveal slight improvements over those previously calculated. However, discrepancies are still apparent along the entire coastline; the maximum discrepancy of 9° is at Clacton.

(ii) Computed phases at continental ports have deteriorated but the maximum discrepancy (13° at Brouwershaven) remains unchanged. Throughout the southern North Sea there is a great density of co-tidal lines. Thus it may be expected that the above phases will generally be quite sensitive to the positioning of the computational points relative to the ports which they represent.
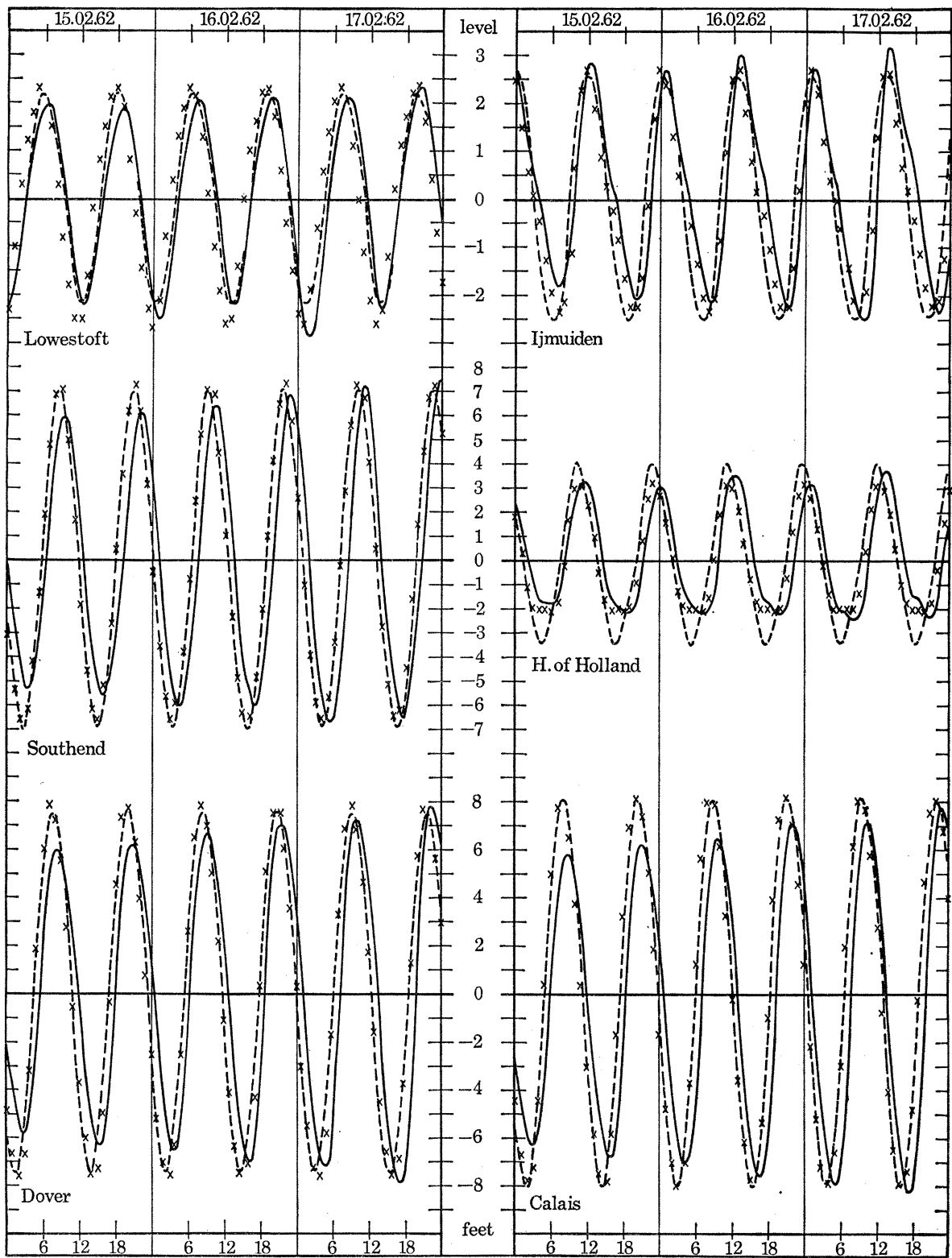
FIGURE 15. Time variations in tidal elevation during 15 to 17 February 1962. ——, total predicted tide; × × ×, predicted lunar tide based on M_2, M_4, M_6; – –, computed lunar tide.

On the whole, the computed amplitudes and phases are improved on the former set.

It now remains to discover to what extent the computed lunar tide for the 15 to 17 February, involving M_2 and its harmonics, approximates to the total astronomical tide for that period. To this end the total tide was determined, using orthodox methods of tidal prediction, at a selection of southern North Sea ports, namely Lowestoft, Southend, Dover, Calais, Hook of Holland and Ijmuiden. Time variations of the total tide, depicted as a continuous curve, are shown in figure 15 alongside the variations of the computed lunar tide depicted as a broken curve. At each port there are pronounced differences in amplitude and phase between the two curves. The phase differences vary slightly over the 3-day period; generally the computed tide is about 1 h in advance of the predicted tide. Differences in amplitude show no definite trend, the computed tide being sometimes greater than and sometimes less than the predicted tide. In the predicted curves the gradual increase in amplitude associated with the neap-spring cycle of the tide is most noticeable at every port and at most ports diurnal tidal variations are also apparent. These effects are neglected in computing the lunar tide which, however, is seen to be a reasonable approximation to the predicted tide.

At Lowestoft, Southend, Ijmuiden and the Hook of Holland the computed tide has the fast rise and slow fall associated with the generation of higher order constituents of the tide in shallow water. Using orthodox methods of tidal prediction the lunar tide consisting of M_2, M_4 and M_6 was determined at each of the chosen southern North Sea ports. A comparison of the computed and this predicted tide is indicated in figure 15 where crosses denote hourly values of the latter. At Dover, Southend and Calais there is good agreement, whereas at the Hook of Holland and Ijmuiden there are marked differences – possibly suggesting that quarter- and sixth-diurnal oscillations have not been adequately generated by the model at these ports. For a general improvement in tidal computations it would be necessary to include these oscillations along the open boundaries and also introduce solar semi-diurnal and as many other constituents of the tide as possible.

5. Computations of tide and surge

Computations were designed to simulate the response of the sea, first to wind stresses alone and subsequently to wind stresses imposed in the presence of a tide. Perturbations of sea level during an actual surge period (15 to 17 February 1962) have been computed and the results verified against observations. Tidal elevations for this period were computed in the last chapter. The present computations of 'surge alone' and 'tide and surge combined' facilitate the study of tide–surge interaction.

(a) Scheme of calculation

Surge conditions are generated throughout the model sea by simulating both the meteorological conditions over the area and the surge elevations along the open boundaries. By simultaneously introducing the tidal oscillations along the open boundaries, the combined effects of tide and surge are produced. Initial conditions of the tidal elevations and currents are required at the beginning of the surge period. As far as surge conditions alone are concerned, the sea is considered to be initially quiescent.

Meteorological conditions over the sea were simulated following the pattern described in §3d. The sea area was divided by parallel 52° 30.5′ N into two sub-areas corresponding to the weather forecasting areas used by the Meteorological Office. It was assumed that the wind

stress was, at any time, uniformly distributed over each sub-area, and for each, values of the wind speed and direction were specified at 2 h intervals. The stress remained constant over each sub-area during every 2 h interval. Wind data at 2 h intervals were available from data sheets already prepared by the Meteorological Office for investigations by Heaps (1969) into North Sea surges. The data had been prepared by extracting geostrophic winds from hourly weather charts and converting these winds to surface winds using a method devised by Findlater *et al.* (1966).
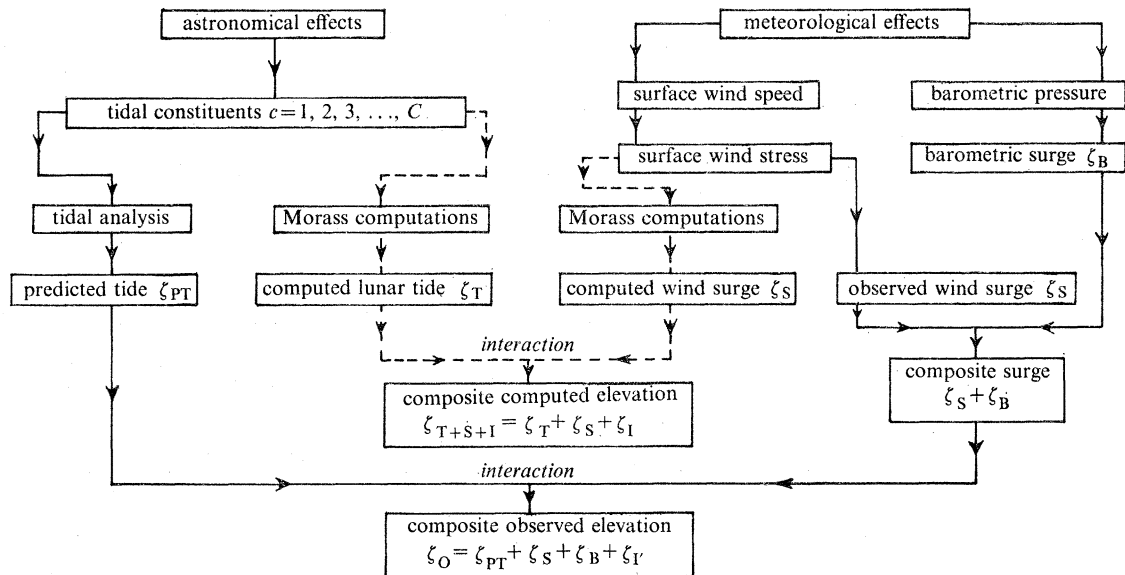

FIGURE 16. Scheme for calculating sea levels. – –, Morass computations.

Elevations representing the head of surge entering the region were specified at each open boundary point at 2 h intervals. Then, as described in §3*d*, interpolation with respect to time yielded elevations at each time step τ. Surge levels computed by Heaps (1969) using a linear model of the North Sea provided input across the Morass open boundaries, taking elevations from Heaps's model along parallels of latitude closest to the Morass boundaries. Because of the larger mesh size of the North Sea model, elevations at intermediate points of the Morass boundary were obtained by graphical interpolation.

The relevance of the model computations to the problem of calculating variations in sea level is shown in figure 16. The observed elevation of sea level, ζ_O, consists of a predicted tidal contribution, ζ_{PT}, a wind-induced surge, ζ_S, a barometric surge, ζ_B, and a tide-surge interaction, $\zeta_{I'}$. The total computed elevation, ζ_{T+S+I}, is limited to contributions from the lunar tide, ζ_T, the wind surge, ζ_S, and the interaction between lunar tide and wind surge, ζ_I. The computed lunar tidal elevation ζ_T is assumed to approximate to tidal elevation ζ_{PT} obtained from orthodox methods of prediction. Both computed and observed elevation of the wind-induced surge ζ_S should be compatible. Also since the majority of interaction in the southern North Sea is between the wind-induced surge and the dominant M_2 tide, computed interaction ζ_I can be assumed to approximate to actual interaction $\zeta_{I'}$. It follows that the total computed elevation ζ_{T+S+I} should be comparable to the observed elevation minus the barometric surge since $\zeta_O - \zeta_B$ ($= \zeta_{PT+S+I'}$ say) $\approx \zeta_{T+S+I}$. Extraction of the tide plus barometric surge from the observed

elevations yields sea level residuals $\zeta_O - \zeta_{PT} - \zeta_B$ ($= \zeta_{S+I'}$), and such levels should be comparable to the computed elevation $\zeta_{T+S+I} - \zeta_T$ ($= \zeta_{S+I}$). Barometric surge ζ_B is estimated from the statical law (Heaps 1967). This law, quoted for example by Charnock & Crease (1957) and Cartwright (1968), gives the surge in terms of the local deviation of barometric pressure from its mean value. No account is taken of dynamic effects produced by changes in barometric pressure over the sea surface.
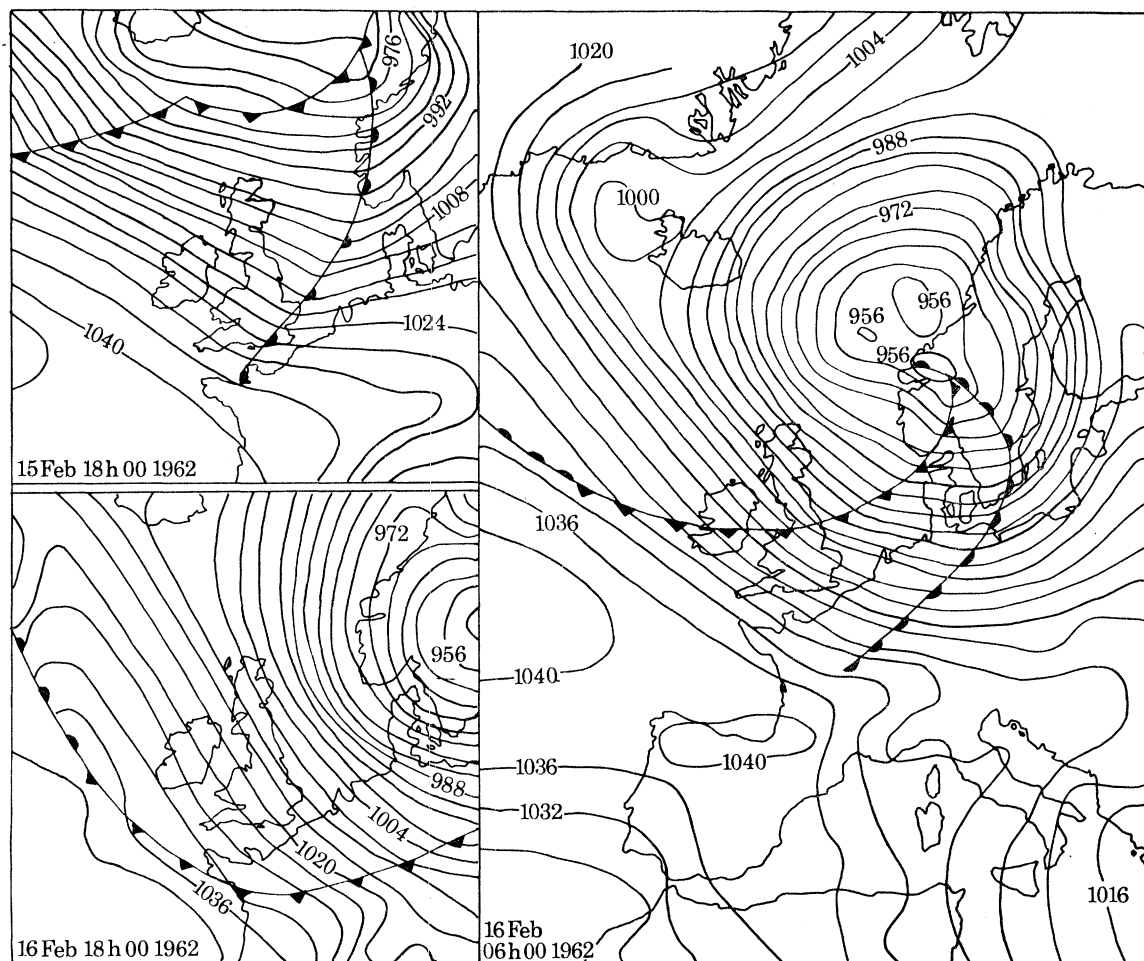

FIGURE 17. Weather charts for the storm surge of 15 to 17 February 1962.

For the surge case considered, comparisons were made between elevations derived from observations at selected ports and computed elevations at grid points in close proximity to the ports. Relative locations of the selected ports and the associated grid points, indicated by double circles, can be seen in figure 14.

The major part of the surge occurred between 00 h 00 on the 15 February and 00 h 00 on 18 February 1962 and was instrumental in raising sea levels to quite extraordinarily high values in the southern North Sea. Along the Dutch coast surge levels of over 7 ft were recorded and in the German Bight levels topped the 11 ft mark. Because of disastrous flooding at Hamburg, the event has come to be known as the 'Hamburg' surge. The responsible meteorological conditions are shown in the weather charts of figure 17.

(b) Surge alone

Each day of the surge period 15 to 18 February 1962 was computed separately so that the recorded average daily freshwater flow into the river at Richmond could be specified. The sea was defined to be initially quiescent, then, following the pattern described earlier in this section, surge elevations along the open boundary, and wind stresses over the model, generated surge levels throughout the 3-day period. Tides were omitted from these calculations.

Variations of wind-induced sea levels are presented in figures 18 and 19. The figures give a comparison of computed and observed surge levels at a selection of ports in the southern North Sea and Thames Estuary. For each of the ports the observed wind-induced level $\zeta_O - \zeta_{PT} - \zeta_B$, depicted by a dot–dashed curve, is presented along with the wind-induced level,
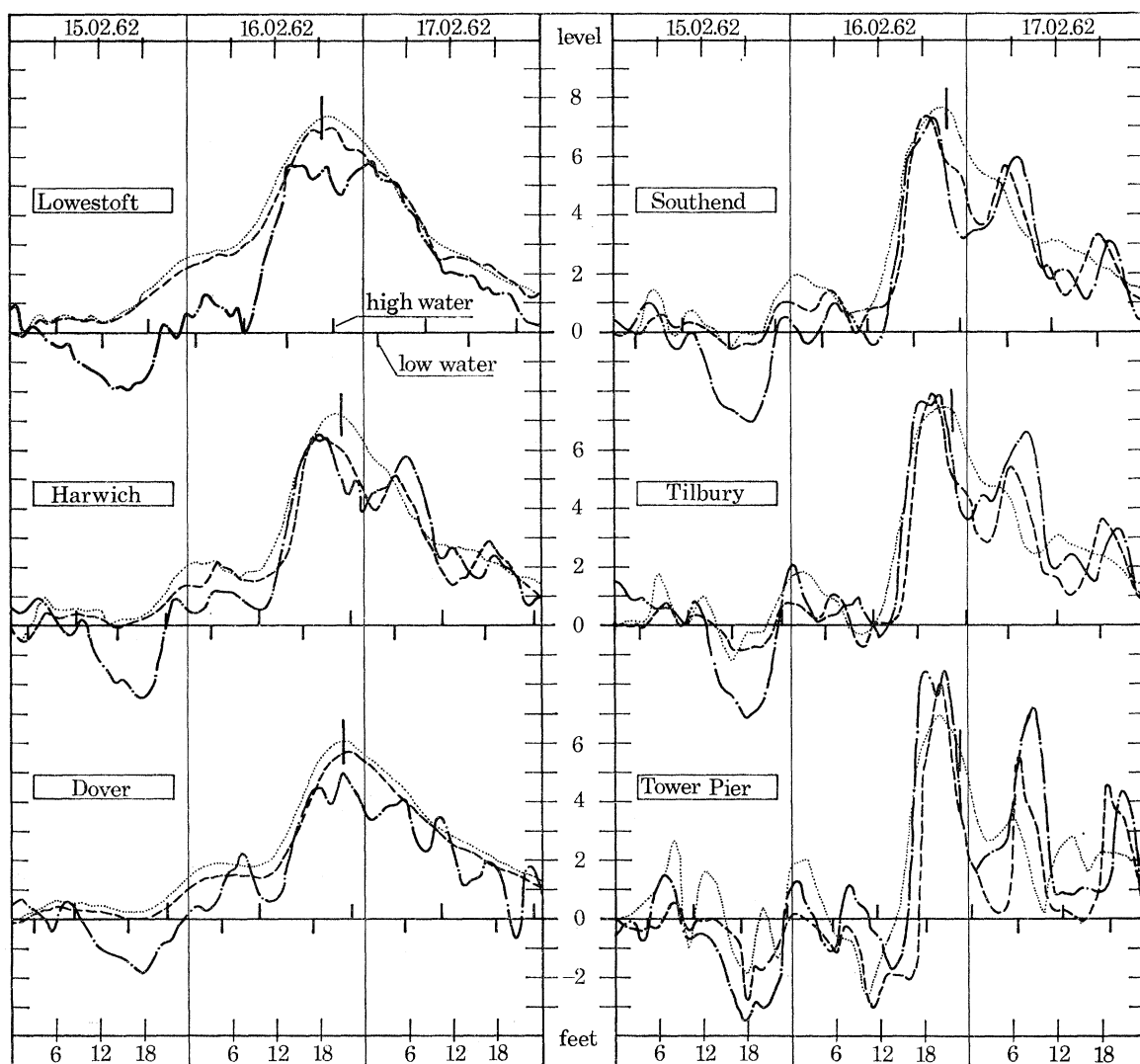

FIGURE 18. Time variations in wind-induced sea levels of the Hamburg surge at British ports. —·—, Observed residual elevation after removal of the barometric surge; – –, surge level ζ_{s+t} computed on the basis of wind and tide; ..., wind surge ζ_s computed in the absence of a tide. Times of high and low water of the total predicted tide are marked along the abscissae. The vertical line near the peak surge corresponds to the time of high water of the computed lunar tide.

ζ_S, computed using Morass, depicted by a dotted curve. Observed surge levels, $\zeta_O - \zeta_{PT} - \zeta_B$, display semi-diurnal type oscillations, particularly so at Harwich, Southend, Tilbury and Tower Pier. Smaller quarter-diurnal-type fluctuations are evident at Ijmuiden, Hook of Holland, Nieuport and Dover. Times of predicted tidal high and low water marked at each port show that in general the peaks of the surge occur on the rising tide and the troughs on the falling tide.
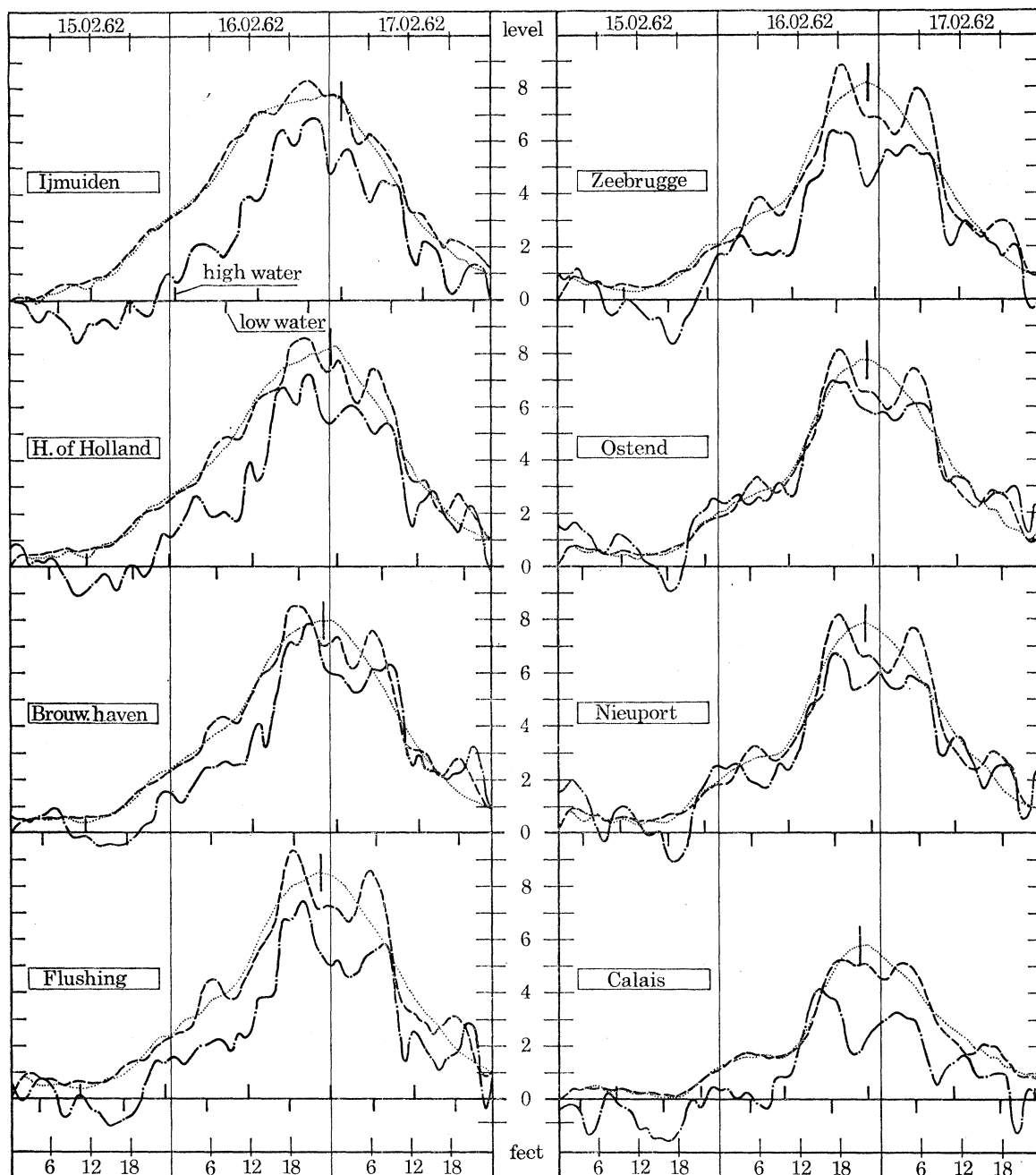

FIGURE 19. Time variations in wind-induced sea levels of the Hamburg surge at continental ports. —·—, Observed residual elevation after removal of the barometric surge; – –, surge level ζ_{S+I} computed on the basis of wind and tide; …, wind surge ζ_S computed in the absence of a tide. Times of high and low water of the total predicted tide are marked along the abscissae. The vertical line near the peak surge corresponds to the time of high water of the computed lunar tide.

The arrival of surge peaks on the rising tide is a common feature of major North Sea surges (Rossiter 1961; Keers 1968).

In presenting the wind-induced sea level, $\zeta_O - \zeta_{PT} - \zeta_B$, it should be mentioned that the barometric surge ζ_B in the southern North Sea, calculated from the statical law, was relatively small during the period considered, in fact negative and numerically less than 0.5 ft during the major part of the surge. The static response of sea level was taken as 1 cm rise for each millibar decrement in atmospheric pressure below the mean (taken here as 1012 mbar).

Surge levels calculated with Morass, without tides, are seen to be in reasonable agreement with observed levels although negative levels occurring during the 15 February are not fully reproduced. In fact the negative surge was not generated within the southern North Sea but originated off the coast of Scotland early on the 15 February and travelled south into the region. The open boundary data for the 15 February did not define the negative surge and hence it was not propagated within the model. Computations covering the remainder of the period were largely successful in reproducing the general rise and fall of the observed surge and it may therefore be reasonably supposed that the mechanism of surge generation in the southern North Sea was satisfactorily reproduced by the model. Calculated surges were generally larger than those actually experienced but tentative explanations for the over-estimates may be put forward as follows. It is possible that the wind-induced levels were substantially decreased in the presence of the tides due to the mutual interaction between tide and surge; thus neglect of interaction could have contributed to the over-estimates. It is also possible that too large an amount of surge energy was retained within the model at the southern open boundary causing over-estimates especially at Dover and Calais. Any extra head of surge retained at the southern boundary would tend to be propagated northwards along the continental coast contributing excessively to the levels at Calais and Ostend. Finally the erection of a closed barrier across the Dutch delta region of the model may have prevented a leakage of surge energy into that region and this, in turn, may have increased surge heights in the vicinity. It should be pointed out that the computations did not exhibit the semi-diurnal and quarter-diurnal fluctuations apparent in the observed curves. At Southend and Harwich nonlinear surge levels show the first traces of the double peaks apparent in the observed surge. This is an improvement over the linear surge computed by Heaps (1969) and is due to the nonlinear effect of surge–surge interaction.

(c) Tide and surge: their interaction

Once again the recorded average daily freshwater flow into the river at Richmond was specified and each day of the surge period was calculated separately. Over the period 15 to 18 February fluctuations of tide and surge within the model were sustained, as described previously in this section, by the simultaneous existence of wind stresses over the model and both linear surge elevations and M_2 tidal oscillations along the open boundaries. The initial conditions of the tide on the 15 February were derived from the earlier tidal computations. Figures 18 and 19 show the variations of ζ_{S+I}, the surge including its interaction with the tide. This is obtained by subtracting the tide ζ_T from the total computed elevation ζ_{T+S+I} as described in §5a.

In progressing from ζ_S to ζ_{S+I} it is important to note the improved agreement with the observed residuals after introducing the interplay with the tides. As well as reproducing the general rise and fall in level, the newly computed residuals have a faster rise to their maximum than the simple wind surges and they also contain the semi- and quarter-diurnal fluctuations introduced through interaction with the tide. The best reproductions of the observations are at Harwich,

Southend (see figure 20), Tilbury and Tower Pier, while at other ports there are discrepancies in the magnitudes and phases of the computed oscillations. Differences between observations and theory are to be expected particularly in rapidly shallowing areas or where the position of the grid point representing a port is considerably displaced from the port itself as in the case of Lowestoft, Brouwershaven, Flushing, Nieuport and Zeebrugge. However, there are also discrepancies in level at Lowestoft, Ijmuiden, Dover and Calais, where levels are influenced by
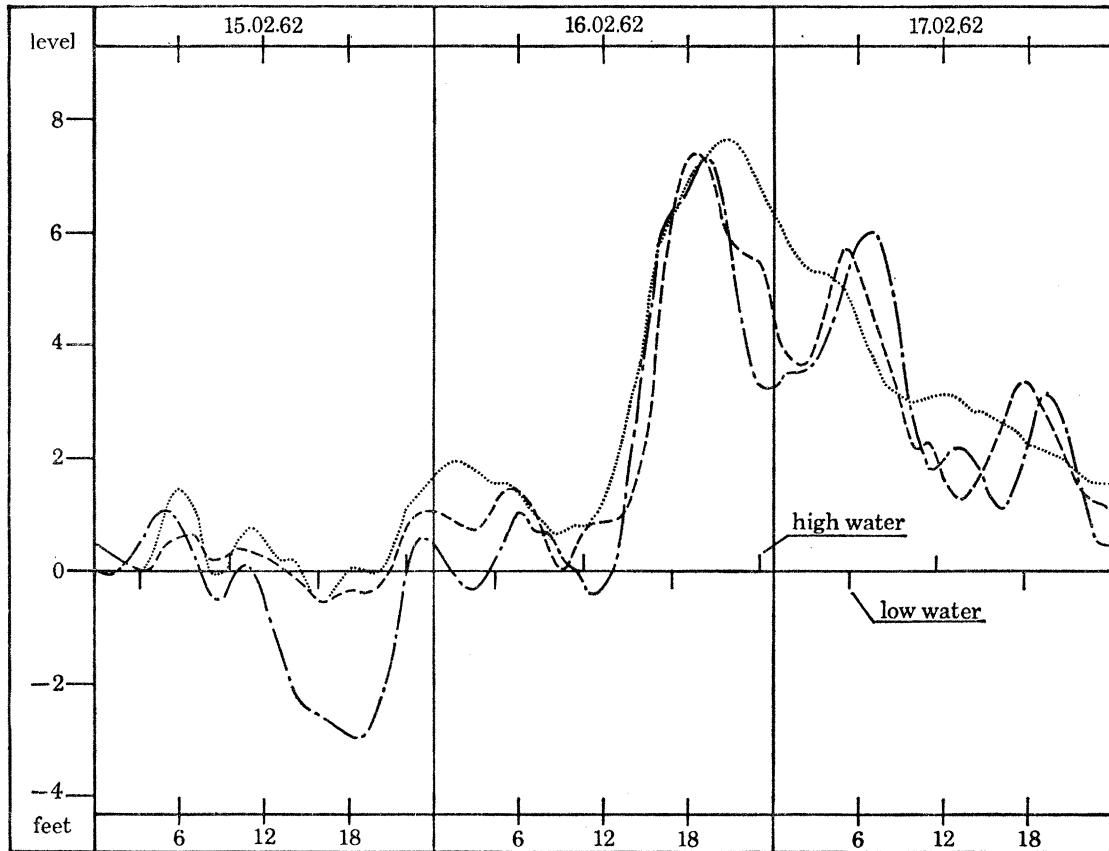

FIGURE 20. Wind-induced surge levels at Southend during the period of the Hamburg surge. $-\cdot-$, Observed residual elevation after removal of the barometric surge; $--$, surge level ζ_{s+I} computed on the basis of wind and tide; ..., wind surge ζ_s computed in the absence of a tide.

the head of surge entering or leaving the region across the open boundaries. In the absence of records from which to define surge levels across open boundaries, the levels were obtained from linear model computations which appear to have over-estimated the true values. Also it must be pointed out that in using linear surge levels along the open boundaries, interaction fluctuations generated outside these boundaries have been omitted. Clearly this could be an important omission responsible for the model's poor reproduction of semi- and quarter-diurnal fluctuations at the above mentioned ports.

Apart from the excess head of surge on the continental coast computed residuals are in good agreement with the observations confirming that the major interaction is simply between the surge and the M_2 tide. The phase discrepancy between the computed and the total astronomical tide did not affect the shape and timing of the residuals. This is possibly because the

wind-induced surge was of much longer duration than the tide and therefore the phases of the actual and computed tides relative to the timing of the surge were not significantly different.

Clearly the effects of tides on surges depend among other things on their phase relationships. At each port shown in figures 18 and 19 the time of high water of the computed lunar tide nearest to the time of maximum wind-induced surge is designated by the short vertical line cutting the latter curve, the phase relationship of the theoretically derived tide and wind-induced surge is therefore apparent. At Lowestoft, Harwich, Southend, Dover and Calais the wind-induced surge peaks occur within a $\frac{1}{2}$ h of lunar tidal high water and the effect of the tide is seen to decrease
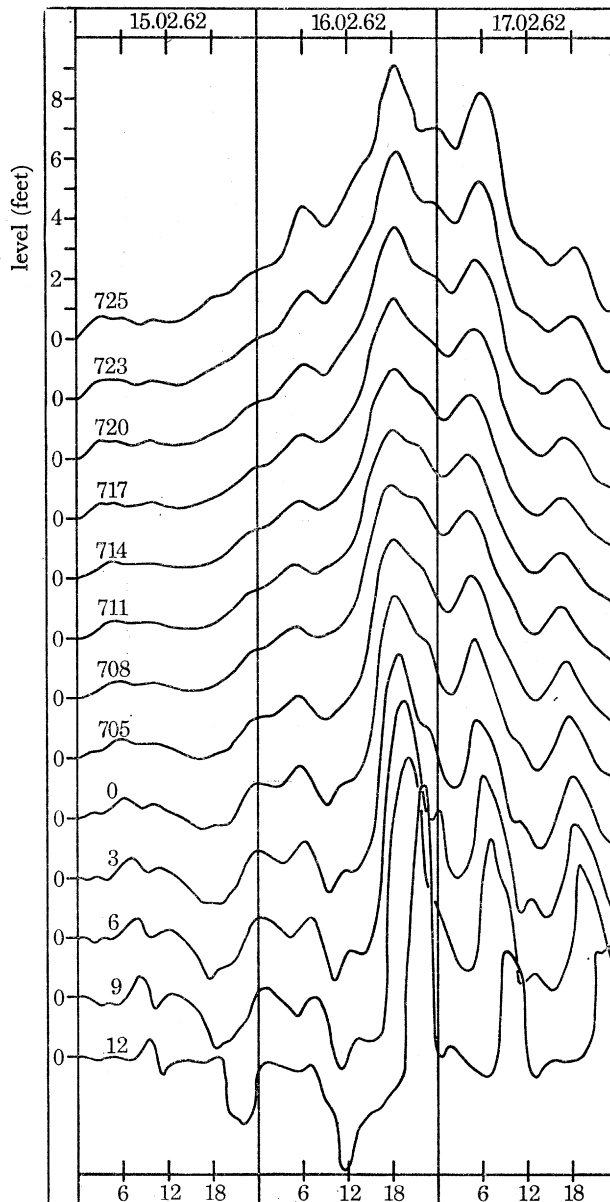

FIGURE 21. Offshore surge residuals, ζ_{S+I}, at points equally spaced along the latitude of the Thames Estuary, extending from section 12 at the head of the estuary outwards across the sea to point 725 on the Dutch coast. Each curve bears the label of the point to which it relates; the exact locations of the points can be seen in figure 14.

the surge residual. This agrees with Proudman's (1955 a) theoretical result for a single progressive wave that, due to friction, the height of a surge whose maximum occurs near to tidal high water is less than that of a surge whose maximum occurs near to tidal low water, the surge maximum decreasing as the range of tide increases. Numerical verification of Proudman's result was obtained by Rossiter (1961), who showed that a surge peak occurring at high water or on the falling tide was decreased in height but (see Tower Pier, Tilbury and Ijmuiden) a peak occurring at low water or on the rising tide was increased in height. In the presence of a progressive wave Proudman further revealed that if a surge has its maximum some time before tidal high water and then remains fairly constant until after tidal high water then, due to friction, the time graph of the surge residual could have two peaks, one occurring before and the other after tidal high water. This effect is clearly seen in the residuals at Nieuport, Ostend, Zeebrugge, Flushing and Brouwershaven.

Computed sea-level disturbances attributable to interaction have proved to be realistic at coastal stations but now model results enable interaction to be inspected at offshore locations where there are no observations. In figure 21 residuals are displayed at equally spaced points along the latitude of the Thames extending from section 12 at the head of the estuary, outward across the sea to a point numbered 725 on the Dutch coast. At each grid point along this latitude double peaks in the surge residuals are most pronounced; off the west coast, at points 705, 708, ..., the fluctuations are mainly semi-diurnal, while traces of quarter-diurnal fluctuations appear in the east (points 723, 725), where the residual heights are greater. The smallest interaction effects are at point 711, where the peak surge first occurs. This is probably related to the arrival of the tide along this latitude, tidal high water first occurring near to point 711 and later to the west and east of the point. Interaction effects increase on either side of the point; also the surge peaks occur progressively later. Travelling inland up the Thames Estuary the general increases in the degree of interaction are consistent with the increasing range of tide, the shallower water and the convergence of the estuary. From figure 21 it is apparent that interaction effects in the southern North Sea are not limited purely to the estuary and coastal belts but spread out laterally into the whole sea region.

Several analytical propositions on the fundamental mechanism of interaction have been confirmed in this brief investigation of the Hamburg surge. Even so it is important to remember that the main virtue of the model does not lie in its analytical capabilities but lies in its power to reproduce actually recorded total sea levels.

6. Concluding discussion

In this paper a mathematical model has been used to reproduce sea levels in the Thames Estuary and the Southern Bight of the North Sea during the period of a major storm. The effects of the tide on surge motion during the storm are of special interest and have been investigated from a theoretical standpoint. The investigation was centred on the Hamburg surge of 15 to 17 February 1962 and involved calculating the response of the sea to (i) the combined effects of tide and wind stress and to the separate effects of (ii) tide alone and (iii) wind stress alone. Eliminating the tidal contribution from sea-level displacements, (i) above, left surge residuals which contained the effects of the tide on the surge. Such interaction effects were clearly revealed through a comparison of the residuals with the wind-induced sea levels, free from tidal influence, obtained from (iii).

The complex nature of interaction phenomena has been demonstrated by Proudman (1955 a, b, 1957) and Rossiter (1961), who respectively performed analytical and numerical studies on the effects of tides on hypothetical surges. In these studies, interaction between a tide and a surge was shown to depend on the type of tidal oscillation, whether standing or progressive, and its phase relationship with the surge. Further, the effect of a tide on a surge is governed by such variables as the range of the tide, the depth of the sea, the effect of bottom friction, the amplitude and duration of the surge and the shape of the time graph of the surge oscillation. In dealing with an actual surge case the interdependence of so many factors complicates attempted descriptions of the interaction. Nevertheless, numerical results for the Hamburg surge have confirmed several conclusions deduced by both Proudman and Rossiter. These results, briefly summarized, are as follows:

(1) For equal sequences of meteorological conditions, wind-induced surge peaks occurring near to the time of tidal high water are decreased in the presence of the tide and peaks occurring on the rising tide are increased. This effect was shown at the British ports considered and agreed with both Proudman's and Rossiter's theoretical results for progressive waves, the effects being attributed to friction. Rossiter explained that a positive surge, increasing the depth of water (a) increases the rate of progression of a free wave and (b) reduces the bottom friction, both factors resulting in a hastening of the tide.

(2) Wind-induced surges rising to a maximum some time before tidal high water and then remaining fairly constant until after tidal high water are, in the presence of the tide, transformed to have two peaks, one occurring before and one after tidal high water. This effect occurred at most continental ports and was in accord with Proudman's findings.

(3) Interaction increases with distance travelled up the Thames. Such increases are consistent with the larger range of tides, the shallower water and the convergence of the estuary.

Theoretical results obtained for the Hamburg surge have only displayed the effects of a tide on a positive surge and there is still scope for further research into the interaction between tides and negative surges. As well as numerical and analytical investigations into this topic, other methods such as response function analysis (Cartwright 1968) and statistical empirical techniques (Keers 1968) are currently being employed to calculate the degree of interaction associated with surges in the North Sea. However, one definite advantage of the mathematical model is its ability to reproduce surge levels throughout an entire sea region. Already in this paper, and possibly for the first time, the knowledge gained of offshore surge residuals has demonstrated the paramount importance of interaction in the southern North Sea; not only did the effect prove to be significant in the very shallow coastal waters but also throughout most of the southern part of the region. The ability of the mathematical model to give an overall reproduction of the total sea-level disturbance due to tide and surge, together with the accuracy of the model computations, has indicated its potential in the field of surge forecasting. Before such forecasts can be made on an operational basis there are several problems including extensions and modifications to the model which should be tackled.

Concerning possible extensions, the area covered by the existing model must be extended into the English Channel in order to take account of meteorologically induced disturbances in the Channel and to reproduce more adequately the propagation of surge energy through the Dover Strait. It would also be an advantage to extend the model northwards so that surges propagated into the Southern Bight would contain the nonlinear effects introduced in the shallow water areas of the Wash. In the rapidly shallowing areas of the model a finer grid might be introduced

to give a more adequate representation of the hydrography and motion in such areas. It is worth while noting that in very shallow areas it may be advisable to modify the bottom friction law in accordance with the surface wind stress; both Reid (1957) and Yamada (1950) found this to be important. A more immediate problem in very shallow water is that of simulating motion in areas of drying banks. If, as in the case of a drying bank, the total depth of water at a grid point of the model becomes zero (i.e. $h + \zeta = 0$), then at that point the equation of motion will contain infinities. A scheme is required which avoids this difficulty by taking account of the moving shoreline.

There is much scope for further improvement in the representation of flow in the Thames Estuary and in the Dutch delta region. In the latter case the major rivers of the delta system should either be given one-dimensional representation or the flow entering and leaving the North Sea through the delta should be specified at the coastal boundary (Leendertse 1967). This is necessary to achieve a more realistic representation of conditions farther north along the Dutch coast. In the case of the Thames Estuary there are two possible improvements. The first is a simple refinement of the specification of flow conditions at Richmond, the head, so that the variations in the flow throughout the day may be reproduced by specifying values at, say, hourly intervals. With regard to the method of calculating estuarine flow a further refinement might be concerned with the reproduction of variations in the longitudinal flow across the estuary. A technique for calculating such variations has been developed by Ramming (1962) and has been shown to improve computations of tidal heights as well as giving a useful display of the time lag between the change from ebb to flood current across any section of the estuary.

Several problems stem from the acquisition of tidal and surge data along open sea boundaries and meteorological data over the region. The problems which have so far been encountered will now be discussed.

Harmonic constituents of the tides at offshore locations are mostly available from co-tidal charts but such charts are generally thought to be unreliable (see §4a) and are usually restricted to the major tidal constituents. In the present work, for simplicity, only M_2 oscillations were specified along the open boundaries generating lunar tides within the model. The simplification gave a satisfactory reproduction of the M_2 tide as was shown by the successful derivation of an M_2 co-tidal chart. However, in computing the lunar tide as an approximation to the total tide, for the Hamburg surge period, it was found that although dominant in the southern North Sea it differed somewhat in amplitude and phase from the total tide. As a consequence it was found that although computed surge residuals were realistic, computed sea levels due to tide and surge were noticeably affected by this limitation on the tide. These results displayed the need, for operational runs of the model, to generate as complete a tide as possible by specifying many more tidal constituents along open sea boundaries.

A possible alternative to specifying tidal constituents at open boundary points would be to specify the sea levels observed at these points. In the absence of observations at offshore locations these could be obtained by interpolating between coastal recordings relating to the ends of the boundaries. Any interpolation would have to reproduce the correct surface gradients across the boundary and this might be aided by the use of tidal current data. If observed levels became available across the open boundaries there would be promise of an improvement in the computed sea levels, open boundary tidal constituents then being determinable.

Open boundary surge levels have so far been obtained from linear model computations for British waters (Heaps 1969). However, an input of tide and linear surge is deficient in its neglect

of interaction at the boundaries. In future the linear surge input should be replaced by an input which contains the effect of the tide on the surge. To obtain the offshore variations in the surge residuals required for such input it would be necessary to employ a nonlinear coarse mesh model of British waters to compute elevations due to both tide and surge. Input for the smaller southern North Sea model could then be obtained from the values thus calculated (Miyazaki 1965). Alternatively, the nonlinear model extending over the whole of the British waters could be arranged so that the coarse grid of the overall sea region surrounded a finer grid covering the southern North Sea. The computations for both grids would then be carried out simultaneously within the same computational array (Jelesnianski 1965). Extending this principle it would be possible to construct a model with a series of nested grids giving a very fine resolution of points in the shallower waters.

Consider now one final problem, that of simulating meteorological conditions over the area. So far the model has only been employed to generate wind-induced surges or surge residuals, the results requiring manual adjustment to account for the effects of the barometric surge. The latter surge is calculated using a statical law which determines the response of the sea to atmospheric pressure. However, there appear to be departures from this law for pressure disturbances of frequency greater than 0.25 c/d owing to the dynamic effects produced in the sea by changes in atmospheric pressure (Cartwright 1968). It is therefore desirable for model calculations to include these dynamic effects by retaining pressure gradients over the sea surface as forcing terms in the equations of motion. To solve the equations it would then be necessary to have a detailed knowledge of atmospheric pressure variations over the sea surface.

Future progress in the operational running of Morass depends on the ready availability of meteorological data in a form suitable for sea-model input. The sea model will require surface wind speeds and atmospheric pressures at grid points over the sea at regular intervals of time. Numerical weather prediction models using very coarse grids compared to the sea model grid are able to supply distributions of atmospheric pressure over the sea surface at regular time intervals; with the advent of finer grid weather models it should become possible to obtain more detailed distributions. It would then remain to convert the output of pressures to yield surface pressures and wind speeds in a form suitable for input to the sea model.

Based on a combined reproduction of tides, wind surges and barometric surge levels Morass results would be directly comparable to observations. Information at specific ports could be deduced from sea levels at adjacent interior grid points of the model. Sea level predictions, like weather forecasting could then become routine.

References

Cartwright, D. E. 1968 A unified analysis of tides and surges round north and east Britain. *Phil. Trans. R. Soc. Lond.* A **263**, 1–55.

Charnock, H. & Crease, J. 1957 North Sea surges. *Sci. Prog., Lond.* **45**, 494–511.

Corkan, R. H. 1948 *Storm surges in the North Sea*, vols I and II. U.S. hydrogr. Off., Misc. 15072, Washington, D.C.

Courant, R., Friedrichs, K. O. & Lewy, H. 1928 Über die partiellen Differenzengleichungen der Mathematischen Physik. *Math. Annln* **100**, 32–74.

Defant, A. 1961 *Physical oceanography*, vol. 2, p. 467. Oxford: Pergamon.

Deutsches Hydrographisches Institut 1963 *Atlas der Gezeitenströme für die Nordsee, den Kanal und die Britischen Gewässer*. Hamburg. 2345.

Doodson, A. T. 1924 Meteorological perturbations of sea level and tides. *Mon. Not. R. astr. Soc. geophys. Suppl.* **1**, 124.

Doodson, A. T. 1928 The analysis of tidal observations. *Phil. Trans. R. Soc. Lond.* A **227**, 230–236.

Dronkers, J. J. 1964 *Tidal computations in rivers and coastal waters*. pp. 191–199. Amsterdam: North Holland Publishing Company.

Findlater, J. *et al.* 1966 Surface and 900 mb wind relationships. *Scient. Pap. met. Off., Lond.* **23**, 1–41.

Heaps, N. S. 1967 Storm surges. *Oceanogr. Mar. Biol. Ann. Rev.* **5**, 11–47.

Heaps, N. S. 1969 A two-dimensional numerical sea model. *Phil. Trans. R. Soc. Lond.* A **265**, 93–137.

Heaps, N. S. & Ramsbottom, A. E. 1966 Wind effects on the water in a narrow two-layered lake. *Phil. Trans. R. Soc. Lond.* A **259**, 391–430.

I.H.B. 1966 International Hydrographic Bureau, Special Publication, 26.

Jelesnianski, C. P. 1965 A numerical calculation of storm tides induced by a tropical storm impinging on a continental shelf. *Mon. Weath. Rev.* **93**, 343–358.

Keers, J. F. 1968 An empirical investigation of interaction between storm surge and astronomical tide on the east coast of Great Britain. *Dt. hydrogr. Z.* **21**, 118–125.

Lauwerier, H. A. 1961 Some recent work of the Amsterdam Mathematical Centre on the hydrodynamics of the North Sea. *Proc. Symp. math.-hydro. methods of phys. oceanography. Mitt. Inst. Meeresk. Univ. Hamburg* **1**, 13–24.

Leendertse, J. J. 1967 Aspects of a computational model for long-period water-wave propagation. *Memo. Rand Corp., Santa Monica, Calif.* RM-5294-PR.

Marineobservatorium Wilhelmshaven 1942 *Karten der Harmonischen Gezeitenkonstanten*, nos. 1802A and 1805A.

Miyazaki, M. 1965 A numerical computation of the storm surge of hurricane Carla 1961 in the Gulf of Mexico. *Oceanogrl Mag.* **17**, 109–140.

Murray, M. T. 1963 The analysis and prediction of tides with a digital computer. M.Sc. Thesis, University of Liverpool.

Otter, J. R. H. & Day, A. S. 1960 Tidal flow computations. *Engineer, Lond.* **209**, 177–182.

Proudman, J. 1953 *Dynamical oceanography*, pp. 17, 45, 162. London: Methuen.

Proudman, J. 1955*a* The propagation of tide and surge in an estuary. *Proc. R. Soc. Lond.* A **231**, 8–24.

Proudman, J. 1955*b* The effect of friction on a progressive wave of tide and surge in an estuary. *Proc. R. Soc. Lond.* A **233**, 407–418.

Proudman, J. 1957 Oscillation of tide and surge in an estuary of finite length. *J. Fluid Mech.* **2**, 371–382.

Quraishee, G. S. 1970 Numerical methods in tidal analysis and prediction. Ph.D. Thesis, University of Liverpool.

Ramming, H. G. 1962 Gezeiten und Gezeitenströme in der Eider. *Proc. Symp. math.-hydro. methods of phys. oceanography. Mitt. Inst. Meeresk. Univ. Hamburg* **1**, 233–237.

Reid, R. O. 1957 Modification of the quadratic bottom stress law for turbulent channel flow in the presence of surface wind stress. *Tech. Memo. Beach Eros. Bd U.S.* **93**, 41.

Richtmyer, R. D. 1957 *Difference methods for initial-value problems*, p. 238. New York and London: Interscience.

Rossiter, J. R. 1959 Research on methods of forecasting storm surges on the east and south coasts of Great Britain. *Q. Jl R. met. Soc.* **85**, 262–277.

Rossiter, J. R. 1961 Interaction between tide and surge in the Thames. *Geophys. J. R. astr. Soc.* **6**, 29–53.

Rossiter, J. R. & Lennon, G. W. 1965 Computation of tidal conditions in the Thames Estuary by the initial-value method. *Proc. Instn civ. Engrs* **31**, 25–56.

Yamada, H. 1950 Theoretical estimation of meteorological high water. *Res. Inst. fluid Engrs* **6**. University of Kyushu.